

**UNIVERSIDAD DE INVESTIGACIÓN DE
TECNOLOGÍA EXPERIMENTAL
YACHAY**

Escuela de Ciencias Químicas e Ingeniería

**TÍTULO: Kinetics of the Oxidative
Dehydrogenation of Polyamines in Iron
Coordination Compounds.**

Trabajo de integración curricular presentado como
requisito para la obtención del título de Químico

Autor:

López Taco Iván Augusto

Tutor:

Ph.D. Saucedo Vázquez Juan Pablo

Químico – López Taco Iván Augusto

Urcuquí, Julio 2020

SECRETARÍA GENERAL
(Vicerrectorado Académico/Cancillería)
ESCUELA DE CIENCIAS QUÍMICAS E INGENIERÍA
CARRERA DE QUÍMICA
ACTA DE DEFENSA No. UITEY-CHE-2020-00025-AD

A los 17 días del mes de abril de 2020, a las 11:30 horas, de manera virtual mediante videoconferencia, y ante el Tribunal Calificador, integrado por los docentes:

Presidente Tribunal de Defensa	Dra. LOPEZ GONZALEZ, FLORALBA AGGENY , Ph.D.
Miembro No Tutor	Dr. SOMMER MARQUEZ, ALICIA ESTELA , Ph.D.
Tutor	Dr. SAUCEDO VAZQUEZ, JUAN PABLO , Ph.D.

El(la) señor(ita) estudiante **LOPEZ TACO, IVAN AUGUSTO**, con cédula de identidad No. **0503182263**, de la **ESCUELA DE CIENCIAS QUÍMICAS E INGENIERÍA**, de la Carrera de **QUÍMICA**, aprobada por el Consejo de Educación Superior (CES), mediante Resolución **RPC-SO-39-No.456-2014**, realiza a través de videoconferencia, la sustentación de su trabajo de titulación denominado: **Kinetics of the Oxidative Dehydrogenation of polyamines in iron coordination compounds**, previa a la obtención del título de **QUÍMICO/A**.

El citado trabajo de titulación, fue debidamente aprobado por el(los) docente(s):

Tutor	Dr. SAUCEDO VAZQUEZ, JUAN PABLO , Ph.D.
--------------	---

Y recibió las observaciones de los otros miembros del Tribunal Calificador, las mismas que han sido incorporadas por el(la) estudiante.

Previamente cumplidos los requisitos legales y reglamentarios, el trabajo de titulación fue sustentado por el(la) estudiante y examinado por los miembros del Tribunal Calificador. Escuchada la sustentación del trabajo de titulación a través de videoconferencia, que integró la exposición de el(la) estudiante sobre el contenido de la misma y las preguntas formuladas por los miembros del Tribunal, se califica la sustentación del trabajo de titulación con las siguientes calificaciones:

Tipo	Docente	Calificación
Miembro Tribunal De Defensa	Dr. SOMMER MARQUEZ, ALICIA ESTELA , Ph.D.	10,0
Tutor	Dr. SAUCEDO VAZQUEZ, JUAN PABLO , Ph.D.	10,0
Presidente Tribunal De Defensa	Dra. LOPEZ GONZALEZ, FLORALBA AGGENY , Ph.D.	10,0

Lo que da un promedio de: **10 (Diez punto Cero)**, sobre 10 (diez), equivalente a: **APROBADO**

Para constancia de lo actuado, firman los miembros del Tribunal Calificador, el/la estudiante y el/la secretario ad-hoc.

Certifico que *en cumplimiento del Decreto Ejecutivo 1017 de 16 de marzo de 2020, la defensa de trabajo de titulación (o examen de grado modalidad teórico práctica) se realizó vía virtual, por lo que las firmas de los miembros del Tribunal de Defensa de Grado, constan en forma digital.*

LOPEZ TACO, IVAN AUGUSTO

Estudiante

**FLORALBA AGGENY LOPEZ
GONZALEZ**

Firmado digitalmente por FLORALBA AGGENY LOPEZ GONZALEZ
Nombre de reconocimiento (DN): c=EC, ou=BANCO CENTRAL DEL ECUADOR,
ou=ENTIDAD DE CERTIFICACION DE INFORMACION-ECIBCE, l=QUITO,
serialNumber=0000269534, cn=FLORALBA AGGENY LOPEZ GONZALEZ
Fecha: 2020.07.08 17:06:55 -05'00'

Dra. LOPEZ GONZALEZ, FLORALBA AGGENY , Ph.D.

Presidente Tribunal de Defensa

**JUAN PABLO
SAUCEDO
VAZQUEZ**

Firmado digitalmente por JUAN PABLO
SAUCEDO VAZQUEZ
Nombre de reconocimiento (DN): c=EC,
o=BANCO CENTRAL DEL ECUADOR,
ou=ENTIDAD DE CERTIFICACION DE
INFORMACION ECIBCE - QUITO,
serialNumber=000260799, cn=JUAN
PABLO SAUCEDO VAZQUEZ
Fecha: 2020.04.17 13:48:07 -05'00'

Dr. SAUCEDO VAZQUEZ, JUAN PABLO , Ph.D.
Tutor

ALICIA ESTELA
SOMMER MARQUEZ

Firmado digitalmente por ALICIA
ESTELA SOMMER MARQUEZ
Fecha: 2020.04.17 14:04:30 -05'00'

Dr. SOMMER MARQUEZ, ALICIA ESTELA , Ph.D.
Miembro No Tutor



Firmado electrónicamente por:
**ANA MARIA
ESCOBAR
LANDAZURI**

ESCOBAR LANDAZURI, ANA MARIA
Secretario Ad-hoc

AUTORÍA

Yo, **Iván Augusto López Taco**, con cédula de identidad 0503182263, declaro que las ideas, juicios, valoraciones, interpretaciones, consultas bibliográficas, definiciones y conceptualizaciones expuestas en el presente trabajo; así cómo, los procedimientos y herramientas utilizadas en la investigación, son de absoluta responsabilidad del autor del trabajo de integración curricular. Así mismo, me acojo a los reglamentos internos de la Universidad de Investigación de Tecnología Experimental Yachay.

Urcuquí, Julio 2020.



Iván Augusto López Taco

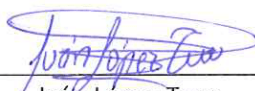
CI: 0503182263

AUTORIZACIÓN DE PUBLICACIÓN

Yo, **Iván Augusto López Taco**, con cédula de identidad 0503182263, cedo a la Universidad de Investigación de Tecnología Experimental Yachay, los derechos de publicación de la presente obra, sin que deba haber un reconocimiento económico por este concepto. Declaro además que el texto del presente trabajo de titulación no podrá ser cedido a ninguna empresa editorial para su publicación u otros fines, sin contar previamente con la autorización escrita de la Universidad.

Asimismo, autorizo a la Universidad que realice la digitalización y publicación de este trabajo de integración curricular en el repositorio virtual, de conformidad a lo dispuesto en el Art. 144 de la Ley Orgánica de Educación Superior

Urququí, Julio 2020.



Iván López Taco

CI: 0503182263

Dedicatoria

A mis padres Iván y Noemí por cada consejo brindado, por cada lágrima secada, por su apoyo y amor incondicional, y más que nada por ser el pilar fundamental en mi vida.

A mi hermano Pablo por estar siempre presente y ser mi cómplice en todo momento.

A mis abuelos, por ser mis segundos padres, por enseñarme a ver la vida de una manera positiva y que a pesar de las adversidades siempre se puede seguir luchando.

Iván Augusto López Taco

Agradecimiento

A Juan Pablo Saucedo por permitirme trabajar junto a él en esta laboriosa investigación, por su guía y consejos brindados durante este largo camino académico en el transcurso de mi carrera como Químico.

A Flor Alba López y Alicia Sommer por las correcciones y consejos brindados

A Manuel Caetano, Thibault Terencio, Lola de Lima, por la ayuda brindada en el desarrollo de mi investigación.

A la Universidad Yachay Tech por ser el alma mater en mi desarrollo académico.

A los profesores que durante 5 años me enseñaron a amar la ciencia

Abstract

The reactivity of the oxidative dehydrogenation (OD) reactions is influenced by the coordination of the ligands to transition metals. Such oxidative dehydrogenation reactions have been studied for a long time due to their broad participation in chemical and biological systems, and their potential application in the industrial sector, as batteries and alternative energy sources to fossil fuels. Some works on the reaction mechanisms including the activity of molecular oxygen during the reaction process, have been reported before. However some details on these mechanisms and the influence of external oxidants have not yet been fully understood, so further investigation is needed.

In the present work, in an attempt to contribute in somehow to increase the knowledge to the mechanism behind this type of reactions, the synthesis, characterization and results of the study of two oxidative dehydrogenation reactions under oxygen atmosphere (air) are presented. In particular, we worked with two systems composed of two different dipyridinic ligands and a $[\text{Fe}(\text{DMSO})_6](\text{NO}_3)_3$ complex as the iron source. Both dipyridinic ligands are differentiated only by the position of the substitution in the pyridine rings.

Despite the slightly difference between the ligands, it was found that the OD reaction occurs only in one system, this was verified by UV-Vis analysis and by cyclic voltammetry studies of the reaction products between the two ligands with the iron complex. Even more, it was found that the difference in the substitution of the pyridine rings generates a great change in the pKa values for each ligand, which is crucial for the development or not of the oxidative dehydrogenation. Thus, rate constants of different order of magnitude were found for both reactions. This was attributed to the fact that in the system in which OD does not occur, the constant is only influenced by the coordination of the ligand to the transition metal, while for the second system the constant is influenced both by the coordination of the ligand to the metal as well as by the OD process. Finally, the results obtained together with the bibliographic study allowed us to suggest a reaction mechanism for both systems.

Key Words:

Oxidative dehydrogenation, rate constant, IR, NMR, cyclic voltammetry

Resumen

La reactividad de las reacciones de deshidrogenación oxidativa (DO) se ve influenciada por la coordinación de los ligantes a metales de transición. Estas, han sido estudiadas por mucho tiempo debido a su amplia participación en sistemas químicos, biológicos y a su potencial aplicación en el sector industrial como baterías y fuentes de energía alternativas a los combustibles fósiles. En la literatura, se han reportado algunos trabajos sobre los mecanismos de reacción de la DO, incluida la actividad del oxígeno molecular en el mecanismo de reacción, sin embargo, algunos detalles sobre estos mecanismos y la influencia de los oxidantes externos aún no se han entendido completamente, por lo que se necesita más investigación.

En el presente trabajo, en un intento de aportar con un poco de conocimiento al mecanismo detrás de este tipo de reacciones, se presentan la síntesis, caracterización y los resultados del estudio de dos reacciones de deshidrogenación oxidativa bajo una atmosfera de oxígeno (aire). En particular, se trabajó con dos sistemas compuestos de un ligante dipiridínico cada uno y el complejo $[\text{Fe}(\text{DMSO})_6](\text{NO}_3)_3$ como la fuente de hierro, ambos ligantes se diferencian únicamente por la posición de la sustitución en los anillos de piridina para cada ligante.

De manera general, se encontró que la reacción de DO ocurre solo en un sistema, esto se verificó mediante el análisis UV-Vis y mediante estudios de voltamperometría cíclica de los productos de la reacción entre los dos ligantes con el complejo de hierro. Estudios potenciométricos demostraron que la diferencia en la sustitución de los anillos de piridina genera un gran cambio en los valores de pKa para cada ligante, lo que es crucial para el desarrollo o no de la reacción de deshidrogenación oxidativa. Así, se encontraron valores de la constante de velocidad de diferente orden de magnitud para ambas reacciones, esto se atribuyó a que en el sistema en el que no ocurre la deshidrogenación, la constante solo se ve influenciada por la coordinación del ligante al metal de transición, mientras que para el segundo sistema la constante se ve influenciada tanto por la coordinación del ligante al metal así como por el proceso de DO. Finalmente, los resultados obtenidos junto con el estudio bibliográfico nos permitieron sugerir mecanismo de reacción para ambos sistemas.

Palabras clave:

Deshidrogenación oxidativa, constante de velocidad, IR, RMN, voltametría cíclica

Índice.....	1
ABBREVIATIONS.....	5
1. Introduction and justification.....	6
1.1. Reaction mechanisms in inorganic systems.....	6
1.1.1. Types of substitution mechanisms.....	6
1.1.2. Dissociative mechanism (<i>D</i>).....	6
1.1.3. Associative mechanism (<i>A</i>).....	6
1.1.4. Interchange mechanism.....	6
1.2. Substitution reactions in octahedral complexes.....	7
1.3. The <i>trans</i> effect.....	8
1.4. Oxidative dehydrogenation.....	10
1.4.1. Mechanisms of oxidative dehydrogenation in amines.....	11
1.4.1.1. Monoelectronic transfer mechanism.....	11
1.4.1.2. Mechanism of electron pair transfer.....	12
1.4.2. Oxidative dehydrogenation under oxygen atmosphere.....	13
1.4.3. Oxidative dehydrogenation in biochemical systems.....	14
1.4.4. Fuel cells.....	14
2. Problem Statement.....	16
3. Objectives.....	16
3.1. General Objective.....	16
3.2. Specific Objectives.....	16
4. Materials and Methodology.....	17
4.1. List of reagent used.....	17
4.2. Characterization techniques and equipment.....	17
4.2.1. Elemental analysis.....	17
4.2.2. Magnetic Susceptibility.....	17
4.2.3. IR spectroscopy.....	18

4.2.4.	NMR spectroscopy	18
4.2.5.	Electrochemistry analyses.....	18
4.2.6.	UV- Vis spectroscopy	18
4.2.7.	pKa measurements.....	18
4.3.	Methodology	18
4.3.1.	Synthesis of the $[\text{Fe}(\text{DMSO})_6](\text{NO}_3)_3$ complex.....	18
4.3.1.1.	Characterization of the $[\text{Fe}(\text{DMSO})_6](\text{NO}_3)_3$ complex	19
4.3.1.1.1.	Cyclic voltammetry.....	19
4.3.2.	Synthesis of the trichlorohydrate 1,9-bis(2' pyridyl)-2,5,8- triazaanonane ($\text{L}^2 \cdot 3\text{HCl}$).....	19
4.3.2.1.	Characterization of the $\text{L}^2 \cdot 3\text{HCl}$ compound.....	20
4.3.2.1.1.	Determination of the pKa values.....	20
4.3.3.	Synthesis of the trichlorohydrate 1,9-bis(3' pyridyl)-2,5,8- triazaanonane ($\text{L}^3 \cdot 3\text{HCl}$).....	20
4.3.3.1.	Characterization of the $\text{L}^3 \cdot 3\text{HCl}$ compound.....	21
4.3.3.1.1.	Determination of the pKa values.....	21
4.4.	Reaction between $\text{L}^2 \cdot 3\text{HCl}$ and $[\text{Fe}(\text{DMSO})_6](\text{NO}_3)_3$	21
4.5.	Reaction at higher concentration	21
4.6.	Characterization of the $[\text{Fe}^{(\text{II})}\text{L}^4]^{2+}$ complex.....	22
4.6.1.	Cyclic voltammetry	22
4.6.2.	Chemical kinetics of the reaction.....	22
4.7.	Reaction between $\text{L}^3 \cdot 3\text{HCl}$ and $[\text{Fe}(\text{DMSO})_6](\text{NO}_3)_3$	22
4.8.	Reaction at higher concentration	22
4.9.	Characterization of the $[\text{Fe}^{(\text{III})}\text{L}^3]^{3+}$ complex.....	23
4.9.1.	Cyclic voltammetry $[\text{Fe}^{(\text{III})}\text{L}^3]^{3+}$ complex	23
4.9.2.	Chemical kinetics of the reaction.....	23
5.	Results and Discussion	24
5.1.	Synthesis of the complex $[\text{Fe}(\text{DMSO})_6](\text{NO}_3)_3$	24
5.1.1.	Determination of the magnetic susceptibility and effective magnetic moment for the $[\text{Fe}(\text{DMSO})_6](\text{NO}_3)_3$ complex.....	24

5.1.2.	Elemental Analysis of the $[\text{Fe}(\text{DMSO})_6](\text{NO}_3)_3$ complex.	26
5.2.	9-bis(2' pyridyl)-2,5,8- triazaanoneno (L^2)	27
5.2.1.	Synthesis of the trichlorohydrate $\text{L}^2 \cdot 3\text{HCl}$	27
5.2.2.	Infrared spectrum of $\text{L}^2 \cdot 3\text{HCl}$ compound	28
5.2.3.	NMR	28
5.2.3.1.	^1H Nuclear magnetic resonance of $\text{L}^2 \cdot 3\text{HCl}$	29
5.2.3.2.	Coupling constants (J) of $\text{L}^2 \cdot 3\text{HCl}$.	29
5.2.3.3.	^{13}C Nuclear magnetic resonance of $\text{L}^2 \cdot 3\text{HCl}$	30
5.2.3.4.	HSQC Spectrum for the $\text{L}^2 \cdot 3\text{HCl}$ compound	31
5.2.4.	Determination of the pKa values for $\text{L}^2 \cdot 3\text{HCl}$	33
5.3.	1,9-bis(3' pyridyl)-2,5,8- triazanoneno (L^3)	35
5.3.1.	Synthesis of the trichlorohydrated $\text{L}^3 \cdot 3\text{HCl}$	35
5.3.2.	Elemental analysis of the $\text{L}^3 \cdot 3\text{HCl}$ ligand	35
5.3.3.	Infrared spectrum of the $\text{L}^3 \cdot 3\text{HCl}$ compound	36
5.3.4.	NMR	37
5.3.4.1.	^1H Nuclear magnetic resonance of $\text{L}^3 \cdot 3\text{HCl}$	37
5.3.5.	Determination of the pKa values for $\text{L}^3 \cdot 3\text{HCl}$	38
5.4.	Kinetics	40
5.4.1.	Rate constant calculation for the reaction between L^2 and $[\text{Fe}(\text{DMSO})_6](\text{NO}_3)_3$	40
5.4.2.	Kezdy-Swinbourne treatment	42
5.4.3.	UV-Vis spectrum in aqueous solution and diffuse reflectance for the $[\text{Fe}(\text{DMSO})_6](\text{NO}_3)_3$ complex.	46
5.4.4.	Calculation of the rate constant for the reaction between L^3 and $[\text{Fe}(\text{DMSO})_6]^{3+}(\text{NO}_3)_3$	47
5.5.	Cyclic voltammetry	51
5.5.1.	Cyclic voltammetry for the $[\text{Fe}(\text{DMSO})_6](\text{NO}_3)_3$ complex in aqueous medium	51
5.5.2.	Cyclic voltammetry for the $[\text{Fe}^{\text{II}}\text{L}^4]^{2+}$ complex in aqueous medium	52
5.5.3.	Cyclic voltammetry for the $[\text{Fe}^{\text{III}}\text{L}^3]^{3+}$ complex in aqueous medium	53
5.6.	Mechanism for the oxidative dehydrogenation reaction between L^2 and $[\text{Fe}(\text{DMSO})_6]^{3+}$	54

5.7.	Mechanism for the oxidative dehydrogenation reaction between L^3 and $[Fe(DMSO)_6]^{3+}$.57
6.	Summary and Conclusion	59
7.	Bibliography	61
8.	Annexes	64
8.1.	Substitution reactions in Square Planar Complexes	64
8.1.1.	Nucleophilic substitution	64
8.2.	Magnetic Susceptibility	65
8.3.	Performance calculations for the yield of complex $[Fe(DMSO)_6](NO_3)_3$ synthesis.	67
8.4.	Data tables for the pKa calculations	67
8.4.1.	$L^2 \cdot 3HCl$	67
8.4.2.	$L^3 \cdot 3HCl$	69

ABBREVIATIONS

List of abbreviations

OD: Oxidative dehydrogenation

NMR: Nuclear Magnetic Resonance

IR: Infrared

UV: Ultraviolet

Vis: Visible

λ : Wavelength

MHz: Megahertz

DMSO: Dimethyl Sulfoxide

LS: Low Spin

HS: High Spin

HSQC: Heteronuclear Single Quantum Coherence

A: Associative

D: dissociative

I_a: Interchange associative

I_d: Interchange dissociative

k_{obs} : Observed rate constant

BM: Bohr Magnetron

1. Introduction and justification

1.1. Reaction mechanisms in inorganic systems

1.1.1. Types of substitution mechanisms

Substitution reactions in inorganic chemistry have been classified in four groups according to the importance of the bond making and breaking in the rate determining step. In inorganic substitutions, the limiting mechanisms are: 1) Dissociative (D), in which the formed intermediate has lower coordination number than the starting complex, and 2) Associative (A) in which the intermediate has a higher coordination number.¹ Dissociative and associative mechanisms involve two step pathways and an intermediate.

1.1.2. Dissociative mechanism (D)

The MX bond is fully broken before the M-Y bond begins to form:



1.1.3. Associative mechanism (A)

The M-Y bond is fully formed before M-X begins to break:



An intermediate occurs at a minimum local energy, it can be detected, and, sometimes isolated. A transition state at a maximum energy, cannot be isolated. In most metal complex substitution pathways, bond formation between the metal and the ligand entering is thought to be concurrent with bond cleavage between the metal and the leaving group. This is known as interchange mechanism (I).¹

1.1.4. Interchange mechanism

In an interchange mechanism there is no intermediate with a coordination number different from that of the starting complex, but there exist various possible transition states:

- Dissociative interchange (I_d), in which bond breaking dominates over bond formation.
- Associative interchange (I_a), in which bond formation dominates over bond breaking.

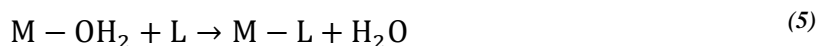
In an I_a mechanism, the reaction rate shows a dependence on the entering group. In an I_d mechanism, the rate shows only a very small dependence on the entering group. It is usually difficult to distinguish between A and I_a , D and I_d , and between I_a and I_d processes.

1.2. Substitution reactions in octahedral complexes

Substitutions in square plane and octahedral complexes are the most common reactions in Coordination Chemistry. A short review on the square plane substitution reaction is presented in Section 8.1. (Annexes) due to the importance of this type of mechanism; however, in our case, we studied substitutions in octahedral complexes and a brief explanation is shown below.

An octahedral complexes substitution may proceed by a D , I_a , I_d or A mechanism and it is often difficult to distinguish between them because, as it was mentioned before, the rate law by itself does not allow a distinction to be made.

For example in the following reaction:



if the reaction follows a dissociative process, the first step would be the breaking of the $M-OH_2$ bond followed by the formation of the $M-L$ bond as follows:



But, the rate equation for this reaction shows a dependence on $[L]$, despite coming from a dissociative mechanism as noted below:

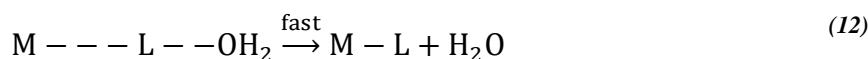
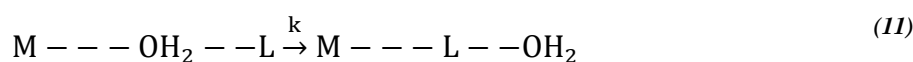
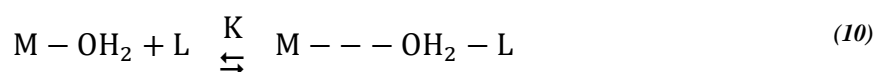
$$-\frac{d[M - OH_2]}{dt} = \frac{k_1 k_2 [M - OH_2] [L]}{k_{-1} [H_2O] + k_2 [L]} \quad (8)$$

At high concentrations of L, $k_2[L] > k_{-1}[H_2O]$ and the last equation can be simplified to a form independent on [L]:

$$\text{rate} = k_{\text{obs}}[M - OH_2] \quad (9)$$

But, at low concentrations of L, both H_2O and L compete for M and the rate shows a dependence on [L]

If some M-L bond making take place before the M-OH₂ bond is completely broken we would be in the presence of an I_d mechanism, the process then would be:



The rate law for this reaction takes the form of a D mechanism:

$$\text{rate} = \frac{kK[M - OH_2][L]}{1 + K[L]} \quad (13)$$

Under pseudo first order reaction this expression simplifies to:

$$\text{rate} = k_{\text{obs}}[M - OH_2] \quad (14)$$

$$\text{with } k_{\text{obs}} = kK[L] \quad (15)$$

The form of the rate law does not change if bond making becomes more important than bond breaking (*I_a*). Since rate laws for *D*, *I_d*, *I_a* and *A* mechanisms cannot be distinguished with certainty, knowledge of the rate and equilibrium constants for individual reaction steps may provide some clarification.

1.3. The *trans* effect

The *trans* effect has been extensively studied in substitution reactions in both square plane and octahedral complexes. By varying the nature of these ligands immense changes in the rate reaction can be achieved, and even more its effect is used to prevent or achieve the synthesis of compounds. So, it is the effect of a coordinated group upon the rate of substitution reactions of ligands opposite to it.²

There are two theories of the *trans* effect, one based on the σ -bonding, and another on the effects of the π -bonding. Both effects contribute to the overall influence of a ligand on the properties of the *trans* M-L bond in square-planar complexes, although the π -*trans*-effect mechanism discussed here is not applicable to octahedral complexes.³

σ -*trans* effect: the σ -*trans* effect or polarization theory considers the *trans* effect to be principally electrostatic and transmitted through σ -bonds. Let's suppose two ligands *F* and *L*, with *L* being in a position *trans* to *F*, and *F* being more polarizable. If a ligand is more polarizable than another this results in the formation of a dipole moment, which means that the electronic distribution will move through the sigma bonds in the direction of the *trans* ligand (*L*). This, usually weakens the M-L bond. Since the polarizability of the metal ion is important, this theory readily accounts for the observation that the *trans*-effect is greatest in the most polarizable or softest metals.

π -*trans* effect: In the π -*trans* effect theory for square-planar complexes, ligand A (Fig. 1) with an empty orbital of π -symmetry can withdraw some of the electron density in the metal d_{xz} orbital away from the *trans*-ligand (*L*). This will have little influence on the ground-state properties of the M-L bond unless that bond also involves π -bonding. In a square-planar complex this will firstly direct an incoming nucleophile towards *L*, which is the region of lowest electron density, and secondly, stabilize the trigonal-bipyramidal transition state since A, *L*, and the incoming ligand all lie in the trigonal plane where A can be most effective at delocalizing the extra charge from the metal.

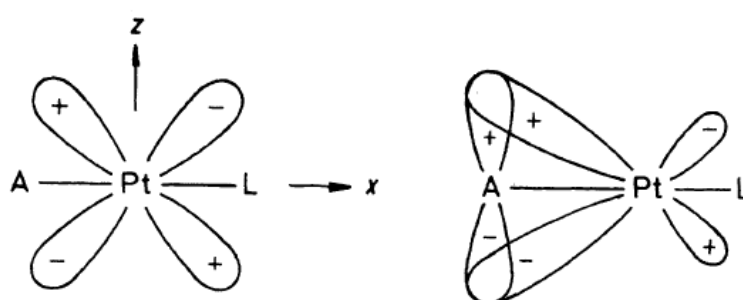


Fig. 1 Representation of the π -bonding mechanism for the *trans* effect taken from The Cis- and Trans- Effects of Ligands³.

1.4. Oxidative dehydrogenation

For many years, oxidative dehydrogenation (OD) reactions have been studied extensively due to their participation in chemical⁴ and biological⁵ systems, and their importance as potential fuel cells through the oxidation of simple alcohols such as methanol.⁶

OD are a type of reaction that generates unsaturations in organic compounds. In alcohols and amines, the nature of the product obtained and its formation rates are influenced by its coordination to transition metals and the nature of the ligand. In this reaction, for amines, quantitative formation of M-N=C type bonds is observed (Fig. 2) and the formation of a variety of products including nitriles, nitro species and carbonyl compounds formed by cleavage reactions of highly reactive imine species formed in the oxidation. In alcohols, aldehydes are produced from primary alcohols and ketones from secondary alcohols.⁷

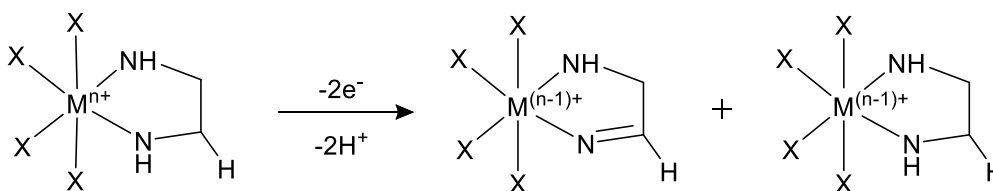


Fig. 2 Representation of the loss of two protons and two electrons in OD reactions.⁸

In Fig. 2 the general scheme of an oxidative dehydrogenation reaction for a bidentate amine under oxygen exclusion is observed. The reaction (OD) involves the loss of two electrons and two protons to form the imine type bond and causes a dismutation reaction with two products, one in which the imine type bond is formed in the ligand (oxidation), while in the other the ligand has not undergone any change.

OD reactions have been studied since the sixties since the development of macrocyclic ligands⁷, due to the constant observation of the conversion of secondary amines to azomethine linkages. In 1966 and 1968 Curtis and his co-workers^{7,9} reported the oxidation of Ni(II) macrocycles (Fig. 3) using nitric acid as an oxidizing agent. At first, it was suggested that this reaction involves high oxidation states of the metal due to the sensitivity of the reaction to the identity of the metal ion. Thus, for example, using Fe(II) as the metal center, the reaction occurred under medium oxidizing conditions, with Ni(II) and Co(II) for the reaction to take place, stronger oxidizing agents were required, and with Co(III) for which there is no high oxidation state easily accessible the oxidation reaction was inert.

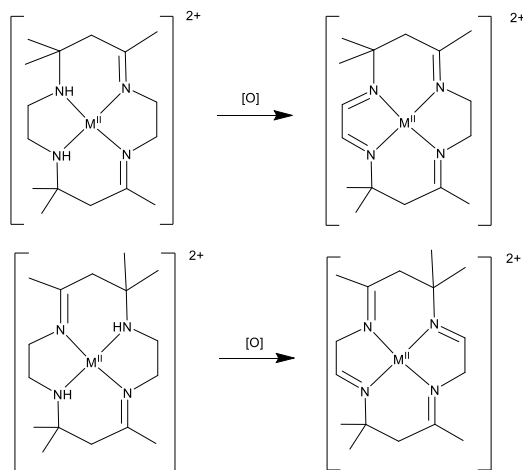


Fig. 3 OD of macrocyclic ligands coordinated to Ni reported by Curtis.

His electrochemical studies were consistent with this hypothesis. For example he showed two-electron electrochemical oxidation of the Cu(II) macrocycle, shown by polarographic and cyclic voltammetric data indicated the involvement of a Cu(III) species.

1.4.1. Mechanisms of oxidative dehydrogenation in amines

OD begins with the one-electron oxidation of the metal center. However, the mechanism of the subsequent intramolecular redox reaction (in which the ligand is oxidized and the metal reduced) is ambiguous, it may take place either by one-electron steps through a ligand-radical intermediate, or involve higher oxidation states of the metal so that alternative two-electron pathways are possible.⁸

1.4.1.1. Monoelectronic transfer mechanism

This mechanism of OD implies the intramolecular transfer of an electron from the coordinated (deprotonated) ligand to the oxidized metal center, which implies the formation of free intermediate radicals.

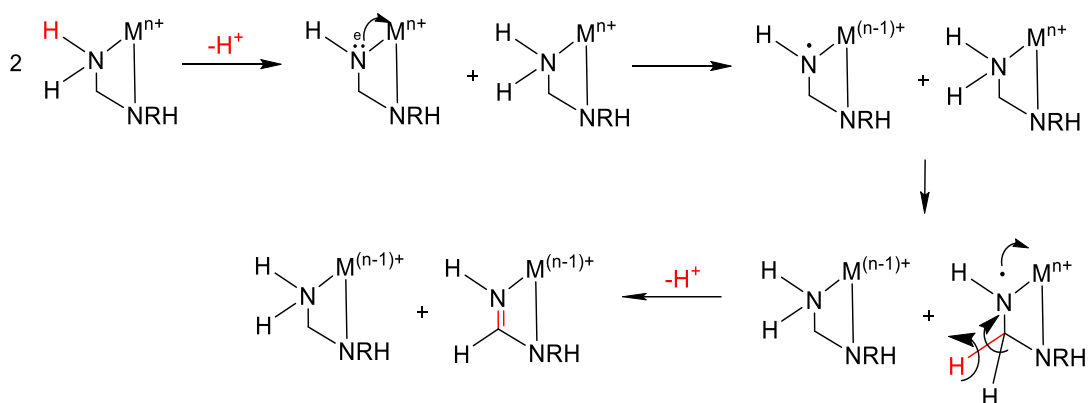


Fig. 4 OD mechanism through mono-electronic transfers.¹⁰

Fig. 4 shows the consecutive intramolecular mono-electronic transfer of the amine coordinated to the metal, coupled with proton removal. This generates a disproportionation reaction with the reduced metal coordinated to the imine ligand and to the unchanged ligand.

1.4.1.2. Mechanism of electron pair transfer

This OD mechanism involves the disproportionation of the oxidized metal center allowing the transfer of electron pairs from the ligand to the metal in the process of dehydrogenation of the ligand. It can happen in two ways: a) By extracting one proton with the subsequent transfer of two electrons from the ligand to the metal center. b) Through a simultaneous transfer of a proton and two electrons.¹¹⁻¹²

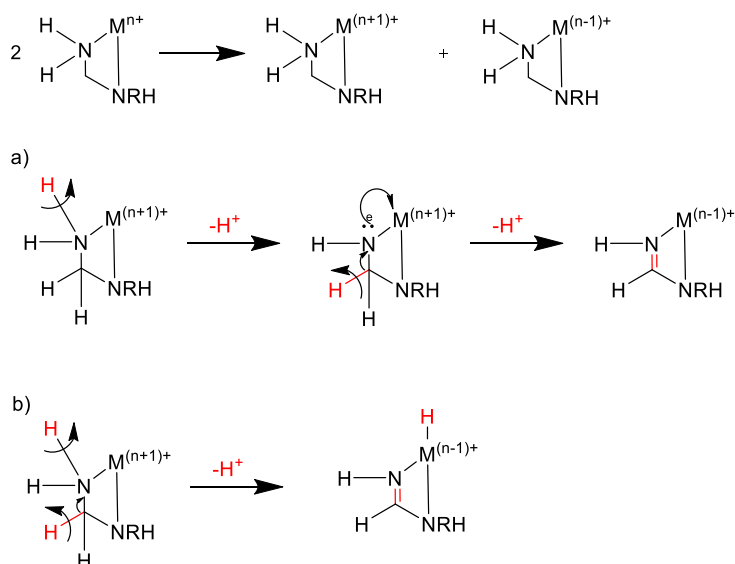


Fig. 5 OD mechanism through electron pair transfer: a) extracting two protons with the subsequent transfer of two electrons from the ligand. b) simultaneous transfer of a proton and two electrons.¹²

1.4.2. Oxidative dehydrogenation under oxygen atmosphere

In 2015, Sosa Torres group¹³ reported a study with a hexadentate ligand $L^3 = 1,9\text{-bis}(2'\text{-pyridyl})\text{-5-}[(\text{ethoxy-}2''\text{-pyridyl})\text{methyl}]\text{-}2,5,8$ triazanone coordinated to Iron (III) $[\text{Fe(III)}L^3]^{3+}$ that was oxidized to the corresponding imine $L^4 = 1,9\text{-bis}(2'\text{-pyridyl})\text{-5-}[(\text{ethoxy-}2''\text{-pyridyl})\text{-methyl}]\text{-}2,5,8\text{-triazanon-1-ene}$ in the final compound $[\text{Fe(II)}L^4]^{2+}$ (Fig. 6). In this reaction, iron changed its oxidation state from 3^+ to 2^+ . It was shown that oxidative dehydrogenation did not occur at an acidic pH while at a neutral or basic pH the reaction favored the formation of the final complex.

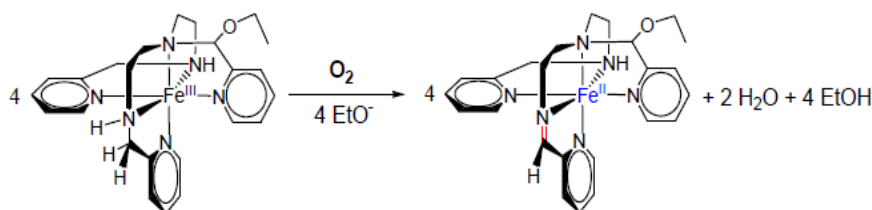
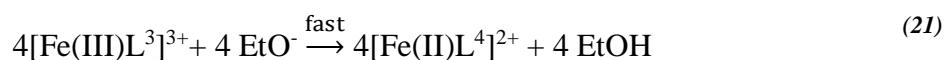
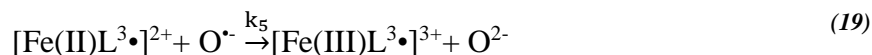
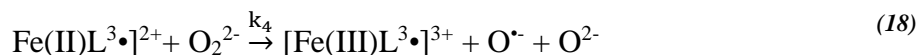
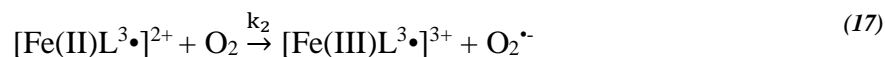


Fig. 6 OD reaction of the $[\text{Fe}^{\text{III}}L^3]^{3+}$ compound under O_2 taken from.¹³

The OD of the ligand (L^3) under oxic conditions suggests a reaction that involves a mechanism of mono-electronic transfer in which at first, the solvent extracts a proton from L^3 coordinated to the transition metal, and this triggers the intramolecular transfers of electron between the transition metal and the coordinated ligand forming radical species centered on the ligand. They show that oxygen participates in the electron transfer forming reduced species that become effective oxidants crucial to the electron transfer process:

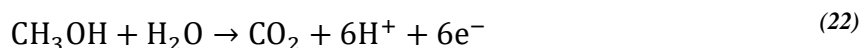


1.4.3. Oxidative dehydrogenation in biochemical systems

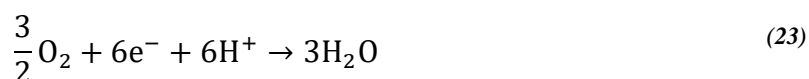
An example of an OD reaction in biochemical system is the one studied by Drif and coworkers¹⁴ about the Catalytic oxidative dehydrogenation of malic acid to oxoacetic acid (OAA). Here, they mention that the conversion of malic acid to OAA is very difficult because the latter is thermodynamically unstable and decarboxylates to pyruvic acid rapidly. Moreover, there is no catalytic route capable of selectively synthesizing OAA from malic acid, so finding a route that allows to stop the oxidation of malic acid to OAA is still a challenge for science. In their study, they found that the dehydrogenation of malic acid was thermodynamically unfavorable, which indicated that the hydrogen produced *in situ* should be quickly converted to turn the reaction towards obtaining the OAA. Thus, they focused on a catalyst (Pt/Bi-C) which was capable of achieving oxidative dehydrogenation of alcohols in addition to hydrogen adsorption to produce water. Thus, they thought that the *in situ* conversion of H₂ to H₂O using the catalyst should move the reaction towards obtaining OAA, and they included to the test. At the end of their investigation and after several tests with the catalyst, they achieved a maximum yield of 60% by selectively converting malic acid into OAA without the detection of products obtained from its subsequent oxidation such as oxalic or pyruvic acid.

1.4.4. Fuel cells

As mentioned earlier, the OD is capable of oxidizing alcohols. A reaction that has taken great interest in recent years is the electro-oxidation of methanol, in principle due to its potential application as a substitute for highly polluting fuels, that is based on the direct methanol fuel cell (DMFC)⁶ (Fig. 7). It consists of an anode at which methanol is electro-oxidized to CO₂ through the reaction:



and a cathode at which oxygen (usually as air) is reduced to water or steam



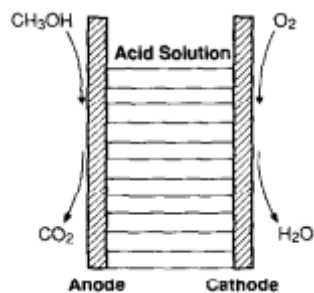


Fig. 7 General scheme of a DMFC taken from⁶.

Moreover, the electrocatalytic OD with catalyzers has been study for their potential application in the production of non-fossil dependent batteries due to the hydrogen production from the oxidation of the substrates is related to the reversible generation of electric current by means of the protons and electrons that are released by the reaction according to the equation:



A clear example of the importance of searching for energy sources that are capable of replacing fossil fuels is the 2019 Nobel Prize awarded to John B. Goodenough, M. Stanley Whittingham and Akira Yoshino for their research on the creation and improvement of lithium ions batteries. These, in their more conventional structure, contain a cathode composed of a lithium metal oxide, a graphite anode, and as an electrolyte a solution of lithium salt in a mixed organic solvent wrapped in a separator filter.¹⁵

2. Problem Statement

As mentioned before, oxidative dehydrogenation reactions have been widely studied due to their participations in chemical and biological systems and due to their potential application in industrial fields like the production of non-fossil dependent batteries. However, all the chemistry behind this type of reaction is not yet fully understood, which is why further studies are still necessary. In an effort to provide knowledge regarding its mechanism through kinetics, the present work studies a new oxidative dehydrogenation system making modifications in previously studied amine ligands, while seeking to generate more efficient systems for selective oxidation of amines under softer reaction conditions, and friendly to the environment using water as the reaction medium.

3. Objectives

3.1. General Objective

The main objective of the present work is to evaluate the reactivity of Fe^{3+} against two pyridinic ligands substituted in different positions.

3.2. Specific Objectives

- To perform the synthesis of two pyridinic ligands substituted in positions 2 and 3.
- To characterize the ligand using conventional techniques (NMR, IR, elemental analysis).
- To study the reaction kinetics of the synthesized ligands using $[\text{Fe}(\text{DMSO})_6](\text{NO}_3)_3$ complex as the source of iron.
- To characterize the reaction products between the ligands and the iron complex using techniques of cyclic voltammetry and UV-Vis spectrophotometry.

4. Materials and Methodology

4.1. List of reagent used

In table 1, the list of the reagents used, together with their purity are mentioned

Table. 1 List of reagent used.

Fe(NO ₃) ₃ •9H ₂ O (Fisher Chemical)	3 pyridine carboxaldehyde (98% Aldrich)
DMSO (99.9%.Sigma-Aldrich)	BufferSolutions (Hach)
[Fe(DMSO) ₆](NO ₃) ₃	Distilled water
2 pyridine carboxyaldehyde (99% Aldrich)	NaNO ₃ (Merck KGaA)
Diethylenetriamine (99%.Sigma-Aldrich)	Glacial acetic acid (100%. Merck KGaA)
LiOH (98% Merck KGaA)	Methanol (Merck KGaA)
NaOH (Merck KGaA)	Hexane (Fisher Chemical)
Iodine	Chloroform (Merck KGaA)
Pd/C (10%.Aldrich)	

4.2. Characterization techniques and equipment

4.2.1. Elemental analysis

These analyzes were carried out in an Analyzer Perkin Elmer CNHS / O series II model 2400 in order to obtain the percentages of carbon, hydrogen and nitrogen with a cystine standard. So the experimental percentage of these elements can be obtained and compared with their theoretical values to see if we are in the presence of the desired compound.

4.2.2. Magnetic Susceptibility

Magnetic susceptibility measurements were made at room temperature by means of a magnetic susceptibility balance, from Evans Johnson-Matthey model. The samples, previously ground, were packed perfectly in thin quartz tubes. The equipment was calibrated using an Cu(Ac₂O) reference standard (NCS). Details about magnetic susceptibility are presented in the section 8.2. (Annexes)

4.2.3. IR spectroscopy

The analysis was performed at room temperature on an IR Agilent Cary 630 FTIR model in a wave number range from 300 to 4000 cm^{-1} at 32 scans with a resolution of 4 cm^{-1} . An ATR sampling technique of the same mark was used on a -1-Bounce diamond crystal.

4.2.4. NMR spectroscopy

NMR resonances of proton (^1H), carbon 13 (^{13}C) and two-dimensional COSY and HSQC experiments were carried out with a 9.4 T Spectrometer Brand Varian Model MR, at 400 MHz.

4.2.5. Electrochemistry analyses

Cyclic voltammetry measurements were performed on an Autolab Metrhom potentiostat-galvanostat equipped with a 3 electrode system.

4.2.6. UV- Vis spectroscopy

UV-Vis and diffuse reflectance spectra were performed on a Perkin Elmer UV / Vis / NIR Spectrometer Lambda 1050 device coupled with quartz cuvettes for aqueous samples.

4.2.7. pKa measurements

pKa was calculated from the titration curves which were performed on a Metler Toledo pH meter Five EasyTMPlus previously calibrated with three buffer solutions at a pH of 4.01 7.01 and 10.01.

4.3. Methodology

4.3.1. Synthesis of the $[\text{Fe}(\text{DMSO})_6](\text{NO}_3)_3$ complex

$[\text{Fe}(\text{DMSO})_6](\text{NO}_3)_3$ complex was made according with the method previously reported¹⁶ with slightly changes. A proportion of 500 mg of $\text{Fe}(\text{NO}_3)_3 \cdot 9\text{H}_2\text{O}$ in 10 mL de DMSO was used for the synthesis. The reaction took place at a temperature (water bath temperature) of 70 °C for an hour. After that time, the reaction change from a brownish red to a yellow-green color, it was an indicative of the product formation. The balloon containing the yellow-green product was let to cool down at room temperature and was immersed in an ice bath during 15 minutes to crystallize the compound, which was recovered by a filtration system and dried for

approximately 45 minutes to ensure that the complex do not contain water. Finally, the compound was weighed and stored for further characterization.

4.3.1.1. Characterization of the $[\text{Fe}(\text{DMSO})_6](\text{NO}_3)_3$ complex

4.3.1.1.1 Cyclic voltammetry

The cyclic voltammetry of $[\text{Fe}(\text{DMSO})_6](\text{NO}_3)_3$ in an aqueous medium was obtained in an Autolab Metrhom Potentiostat-Galvanostat equipped with a three electrode system, in a 0.015 M solution of the complex containing 0.05 M of NaNO_3 as support electrolyte, at a scan speed of 25 mV/s with a 0 to 1 volts window for 3 cycles. The measurements were made using carbon glass as a working electrode, Ag^0 -AgCl as a reference electrode and platinum as a counter electrode.

4.3.2. Synthesis of the trichlorohydrate 1.9-bis(2'pyridyl)-2,5,8- triazaanonane ($\text{L}^2 \cdot 3\text{HCl}$)

The synthesis of the ligand 1.9-bis(2'pyridyl)-2,5,8- triazaanonane trichlorohydrate (Fig. 8) was performed according to the method previously reported¹⁷ with slightly changes using as precursors 2-pyridinecarboxaldehyde and diethylenetriamine in a 2:1 ratio, respectively. 100 mL of ethanol were used as solvent and 0.210 mol of 2-pyridinecarboxaldehyde and 0.105 mol of diethylenetriamine were added. The synthesis was carried at 80 °C with constant stirring. The pH of the solution was monitored during the reaction, observing that this was very basic. Schiff base condensation synthesis occurs in an acid medium, specifically at a pH of 4.5.¹⁸ For this reason, 35.5 mL of 100% glacial acetic acid was added to the solution until the pH of the reaction medium was lowered to about 5. It was observed that as the acid was added, the coloration of the reaction began to change, first to a light green, then to a light yellow, and finally to a light orange color, thus, under these last conditions, it was allowed to continue the reaction for an hour and a half.

To monitor the progress of the reaction, it was used a TLC system using iodine chamber to be revealed. The eluent was composed of methanol, chloroform and hexane in a 1:5:3 ratio. At the beginning two spots were observed corresponding to the amine and the aldehyde compound, where the lower spot corresponded to the amine and the higher spot to the aldehyde. The progress in the synthesis of the ligand was determined qualitatively observing the change in the coloration of the reaction from transparent to orange, characteristic of the pentadentate

ligand, as well as by observing the TLC aldehyde spot disappearance, only remaining the spot corresponding to the diimine. Subsequently, the product from the condensation was placed in a flask connected to a balloon containing H₂ previously generated by the reaction of metallic Zn and HCl¹⁹, and 2 g of 10% Pd/C catalyst were added to undergo hydrogenation at a pressure of 30 psi of H₂ for 4 hours. The catalyst was recovered by filtration through a vacuum system and the obtained solution was bubbled with HCl (g), which was previously got by the Le Blanc reaction process using NaHSO₄ and NaCl¹⁹ to obtain the compound L²•3HCl trichlorohydrate.

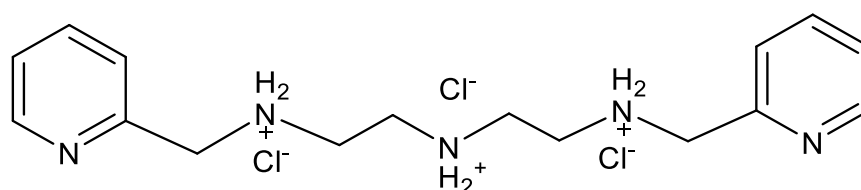


Fig. 8 Representation of the L²•3HCl compound.

4.3.2.1. Characterization of the L²•3HCl compound

4.3.2.1.1. Determination of the pKa values

The titration curve in an aqueous medium for the 1,9-bis(2'pyridyl)-2,5,8- triazaanonane ligand (L²•3HCl) trichlorohydrate was performed by potentiometry. 100 ml of a 0.05 M solution of sodium hydroxide (NaOH) was used as titrant. A 0.0125 M solution of the ligand (L²) in 50 mL of distilled water was prepared. 0.493 g of (L²) were weighed and this mass was introduced into a 50 mL volumetric flask. The flask was capped and gently shaken to ensure total solid dissolution.

The pH meter was calibrated using three buffers at a pH of 4.01, 7.01 and 10.01. In a 200 mL beaker, 50 mL of the 0.0125 M solution of the ligand were placed with a constant stirring. With a graduated burette, intervals of 0.5, 1, 2 and 3 mL of the NaOH solution were dropped and between each interval the pH was measured. This was repeated until the pH stabilized.

4.3.3. Synthesis of the trichlorohydrate 1,9-bis(3'pyridyl)-2,5,8- triazaanonane (L³•3HCl)

The synthesis of the ligand 1,9-bis(3'pyridyl)-2,5,8- triazaanonane trichlorohydrate was performed according to the method previously reported¹⁷ with slightly changes using as

precursors the 3-pyridinecarboxaldehyde and the diethylenetriamine in a 2:1 ratio respectively. 100 mL of ethanol were used as solvent and 0.210 mol of 2-pyridinecarboxaldehyde and 0.105 mol of diethylenetriamine were added. The synthesis was carried at of 80 °C with constant stirring. As before, for this reaction, 45.5 mL of 100% glacial acetic acid were added to the solution to reach the pH = 5. The same changes obtained for the previous ligand synthesis were observed.

Reaction monitoring, the reduction process and the obtaining of the trichlorohydrated ligand ($L^3 \cdot 3HCl$) (Fig. 9) was carried out in the same manner as for $L^3 \cdot 3HCl$.

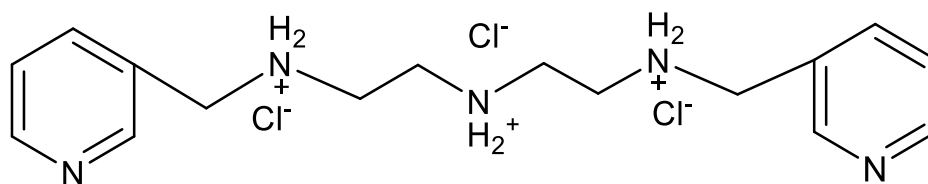


Fig. 9 Representation of the $L^3 \cdot 3HCl$ compound.

4.3.3.1. Characterization of the $L^3 \cdot 3HCl$ compound

4.3.3.1.1. Determination of the pKa values

The titration curve for the 1.9-bis(3'pyridyl)-2,5,8- triazaanonane trichlorohydrate ligand ($L^3 \cdot 3HCl$) was obtained using the same method as for the $L^2 \cdot 3HCl$ compound.

4.4. Reaction between $L^2 \cdot 3HCl$ and $[Fe(DMSO)_6](NO_3)_3$

For the reaction between the $L^2 \cdot 3HCl$ and $[Fe(DMSO)_6]^{3+}$ compounds in aqueous medium, first the trichlorohydrated ligand was neutralized as follows: 2×10^{-4} M solution of the ligand in water was prepared which had an initial pH of 3.88. Then, 3 equivalents of LiOH were added (6×10^{-4} mol), stirred until the solid dissolved completely and the pH was kept constant at 7.01. Then, a solution of 2×10^{-4} M of $[Fe(DMSO)_6](NO_3)_3$ was added and the reaction took place at room temperature with constant stirring for 7.5 hours.

4.5. Reaction at higher concentration

A second reaction between the two previous compounds was carried out following the same methodology but at a concentration of 0.030 M of each substrate. Under this new condition, it was observed that the reaction after 20 minutes took a purple color, such color was reported

before for the OD reaction but in an ethanolic medium¹⁷. This result help us to conclude that the OD reaction happens obtaining the final compound $[\text{Fe(II)L}^4]^{2+}$.

4.6. Characterization of the $[\text{Fe(II)L}^4]^{2+}$ complex

4.6.1. Cyclic voltammetry

The cyclic voltammetry of $[\text{Fe(II)L}^4]^{2+}$ in aqueous medium were obtained in the potentiostat-galvanostat equipped with a three electrode system. Voltammogram of 0.015 M solution of the complex in water containing 0.05 M of NaNO_3 as a support electrolyte was performed under the next conditions: 25 mV/s of scan rate with a -0.8 to 1 volt window for 3 cycles. The measurements were made using carbon glass as a working electrode, Ag-AgCl as a reference electrode and platinum as a counter electrode.

4.6.2. Chemical kinetics of the reaction

The kinetic experiment was performed in an aqueous medium using mixtures of $\text{L}^2 \cdot 3\text{HCl}$ and $[\text{Fe(DMSO)}_6](\text{NO}_3)_3$ in 2×10^{-4} M concentration. First, the ligand was neutralized using three equivalents of LiOH using the pH meter previously calibrated. The initial pH of the solution was 3.88 and after the addition of LiOH it changed to 7.01. The reaction was carried out at room temperature on a round bottom ball with constant stirring. The kinetics experiments were performed following the changes of UV/Vis absorbance in a range from 800 to 190 nm, every 30 minutes during 450 minutes in total.

4.7. Reaction between $\text{L}^3 \cdot 3\text{HCl}$ and $[\text{Fe(DMSO)}_6](\text{NO}_3)_3$

For the reaction between the $\text{L}^3 \cdot 3\text{HCl}$ and $[\text{Fe(DMSO)}_6]^{3+}$ compounds in aqueous medium, first the trichlorohydrated ligand was neutralized, for this, a solution was prepared at a concentration of 2×10^{-4} M of the ligand in distilled water and its initial pH was measured which was 4.01. Then, 3 equivalents of LiOH were added (6×10^{-4} mol) stirred until the solid dissolved completely and then, the pH was measured again which had a value of 7.96. Then, a solution of 2×10^{-4} M of $[\text{Fe(DMSO)}_6](\text{NO}_3)_3$ was prepared. Both solutions were mixed and the reaction took place at room temperature with constant stirring for 5.5 hours. It was not possible to see any change in the color of the reaction, but a precipitate formation was seen almost instantaneously.

4.8. Reaction at higher concentration

A second reaction was performed between the two previous compounds following the same methodology but at a concentration of 0.015 M. However, for this ligand at these conditions it was also not possible to observe the change in the color of the reaction characteristic of the OD process. Moreover, it was seen the formation of an orange precipitate almost instantaneously.

4.9. Characterization of the $[\text{Fe(III)L}^3]^{3+}$ complex

4.9.1. Cyclic voltammetry $[\text{Fe(III)L}^3]^{3+}$ complex

Data for the cyclic voltammetry of $[\text{Fe(III)L}^3]^{3+}$ in an aqueous medium were obtained in the potentiostat-galvanostat equipped with a three electrode system, in water with an unknown concentration because this reaction resulted in a precipitate very difficult to dissolve, so the reaction supernatant was taken to perform the measurement containing 0.05 M of NaNO_3 as a support electrolyte, at a scan rate of 25 mV/s with a 0 to 1 volt window for 3 cycles.

4.9.2. Chemical kinetics of the reaction

The kinetics experiment was performed in an aqueous medium using mixtures of $\text{L}^3 \cdot 3\text{HCl}$ and $[\text{Fe}(\text{DMSO})_6](\text{NO}_3)_3$ in 2×10^{-4} M concentration. First, the ligand was neutralized using three equivalents of LiOH with the help of the pH meter previously calibrated. The initial pH of the solution was 4.01 and after the addition of LiOH it changed to 7.96. The reaction was carried out at room temperature on a round bottom ball with constant stirring. The kinetics were performed following the changes of UV/Vis absorbance in a range from 800 to 190 nm, every 30 minutes for 330 minutes in total.

5. Results and Discussion

5.1. Synthesis of the complex $[\text{Fe}(\text{DMSO})_6](\text{NO}_3)_3$

The synthesis was made according to the experimental section 4.3.1. obtaining a yellow-green compound with a yield of 85.9%. The yield determination can be seen in Section 8.3. (Annexes). Its characterization was made using the techniques of magnetic susceptibility and elemental analysis. A schematic representation of the $[\text{Fe}(\text{DMSO})_6](\text{NO}_3)_3$ is presented below in (Fig. 10).

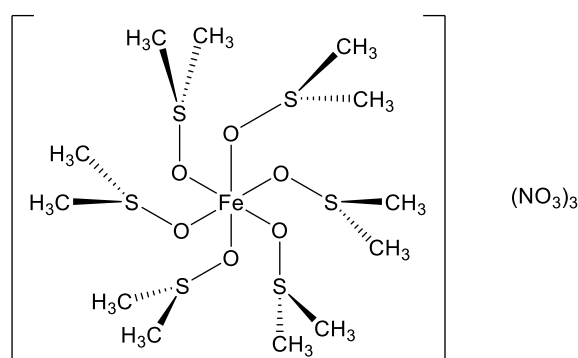


Fig. 10 Representation of the $[\text{Fe}(\text{DMSO})_6](\text{NO}_3)_3$ molecule taken from²⁰

5.1.1. Determination of the magnetic susceptibility and effective magnetic moment for the $[\text{Fe}(\text{DMSO})_6](\text{NO}_3)_3$ complex

For a better understanding a little bit of the magnetic susceptibility theory is resented in section 8.2. (Annexes)

The magnetic susceptibility per gram (X_g) was obtained as follows for the used balance,

$$X_g = \frac{C * h(R - R_0)}{(m - m_0) * 10^9} \quad (25)$$

The following table shows the results and the data used for the determination of the magnetic susceptibility.

Table. 1 Data used for the determination of the magnetic susceptibility.

Parameter	
Compound	[Fe(DMSO) ₆](NO ₃) ₃
C (balance constant)	0.981303
l (sample length)	3.5 cm
m(t ₀) (empty tube mass)	0.67 g
m(t ₀ +M) (tube mass + sample)	0.8847 g
m(M) (sample mass)	0.2147 g
R ₀	-34
R	1202
R-R ₀	1236

Using eq. (25), the magnetic susceptibility per gram was determined

$$X_g = \frac{0.981303 * 3.5 * (1202 + 34)}{(0.8847 - 0.67)g * 10^9} \quad (26)$$

$$X_g = 1.9772 * 10^{-5} \frac{\text{cm}^3}{\text{g}} \quad (27)$$

This is related to molar susceptibility as follows:

$$X_M = X_g * MM \quad (28)$$

where MM is the molar mass of the compound under study, then:

$$X_M = 1.9772 * 10^{-5} \frac{\text{cm}^3}{\text{g}} * 710.66 \frac{\text{g}}{\text{mol}} \quad (29)$$

$$X_M = 0.01405 \frac{\text{cm}^3}{\text{mol}} \quad (30)$$

This susceptibility value will contain the diamagnetic contributions in addition to the paramagnetic contributions, therefore, it is necessary to correct this value taking into account the sum of the diamagnetic contributions, therefore the corrected value would be equal to:

$$X_{\text{corr}} = X_{\text{M}} - \left(\sum \text{diamagnetic correction} \right) \quad (31)$$

The diamagnetic correction for the Fe^{3+} cation, NO_3^- anion: and DMSO are respectively²¹:

$$-10 * 10^{-6} \frac{\text{cm}^3}{\text{mol}}; -18.9 * 10^{-6} \frac{\text{cm}^3}{\text{mol}}; 31 * 10^{-6} \frac{\text{cm}^3}{\text{mol}}$$

Then we have that:

$$X_{\text{corr}} = 0.01405 \frac{\text{cm}^3}{\text{mol}} - \left[\left(-10 * 10^{-6} \frac{\text{cm}^3}{\text{mol}} \right) + 3 \left(-18.9 * 10^{-6} \frac{\text{cm}^3}{\text{mol}} \right) + 6 \left(31 * 10^{-6} \frac{\text{cm}^3}{\text{mol}} \right) \right] \quad (32)$$

$$X_{\text{corr}} = 0.013932 \frac{\text{cm}^3 * \text{emu}}{\text{mol}} \quad (33)$$

The permanent magnetic moment is calculated as follows:

$$(\mu)^2 = \frac{3kTx_{\text{corr}}}{N\beta^2} \quad (34)$$

Where: N = Avogadro's number; β = The Bohr magneton; k = Boltzmann's constant; T = Absolute temperature (K)

Hence:

$$\mu = 2.84 \sqrt{T * x_{\text{corr}}} \quad (35)$$

$$\mu = 2.84 \sqrt{0.013932 \frac{\text{cm}^3}{\text{mol}} * 293.15\text{K}} \quad (36)$$

$$\mu = 5.73 \text{ BM} \quad (37)$$

A molar magnetic susceptibility of $0.01405 \text{ cm}^3/\text{mol}$ was obtained with a permanent magnetic moment (μ) of 5.73 MB which matches with a paramagnetic HS Fe^{3+} molecule.²²

5.1.2. Elemental Analysis of the $[\text{Fe}(\text{DMSO})_6](\text{NO}_3)_3$ complex.

The percentage of carbon, hydrogen and nitrogen present in $[\text{Fe}(\text{DMSO})_6](\text{NO}_3)_3$ was determined. Table. 2 shows the experimental results obtained, these, agree with the theoretical data calculated for the mass percentage of each atom contained in the complex.

Table. 2 Experimental and theoretical elementary analysis of the $[\text{Fe}(\text{DMSO})_6](\text{NO}_3)_3$ compound

Element	Experimental	Theoretical
C	20.43%	20.28 %
H	5.12%	5.11 %
N	5.75%	5.91%
S	27.52%	27.07%
Fe	-----	7.86%
O	-----	33.77%

5.2. .9-bis(2'pyridyl)-2,5,8- triazaanoneno (L^2)

5.2.1. Synthesis of the trichlorohydrate $L^2 \cdot 3\text{HCl}$

The synthesis of the trichlorohydrated $L^2 \cdot 3\text{HCl}$ was performed following the next reaction scheme

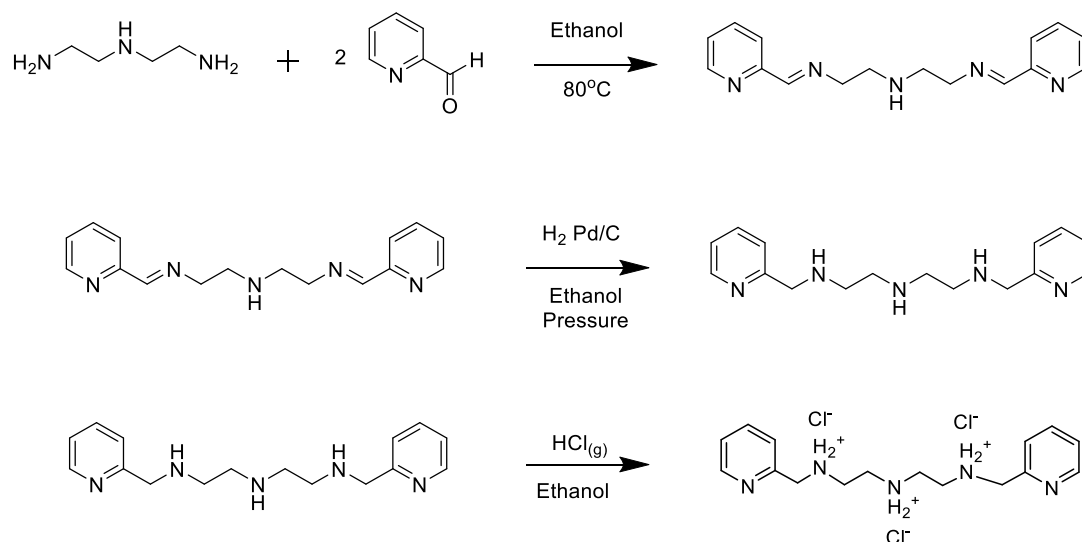


Fig. 11 General scheme of the synthesis of the ligand (L^2) trichlorohydrate.

5.2.2. Infrared spectrum of $L^2 \cdot 3HCl$ compound

The C-H vibration of alkanes is found around 3000 cm^{-1} . The sp^3 C-H absorption, always occurs at frequencies less than 3000 cm^{-1} ($3000\text{-}2840\text{ cm}^{-1}$). Thus, in the infrared spectra (Fig. 12) we have that the bands for $\nu(\text{C-H})$ vibrations of the aliphatic carbons of the (L^2) ligand are at 2983 and 2937 cm^{-1} . The sp^2 absorption, occurs at frequencies greater than 3000 cm^{-1} the bands for $\nu(\text{C-H})$ vibrations of the aromatic carbons at 3041 cm^{-1} . The vibrations corresponding to the $\nu(\text{N-H}_2^+)$ bonds of the protonated amines in the aliphatic chain are found at 2653 , 2556 , 2428 and 2381 cm^{-1} . the $\nu(\text{C=N})$ vibration corresponding to the pyridine rings, is found at 1590 cm^{-1} . Two bands are observed at 1570 y 1459 cm^{-1} for the $\nu(\text{C=C})$ vibration of the pyridine rings. At 1478 cm^{-1} is observed the band corresponding to the $\delta(\text{C-H})$ vibration of the methylenes present in the aliphatic part of the compound. $\delta(\text{C-H})$ oop bending are present at 814 and 755 cm^{-1} resulting from strong coupling with adjacent hydrogens atoms for the monosubstitution pattern.

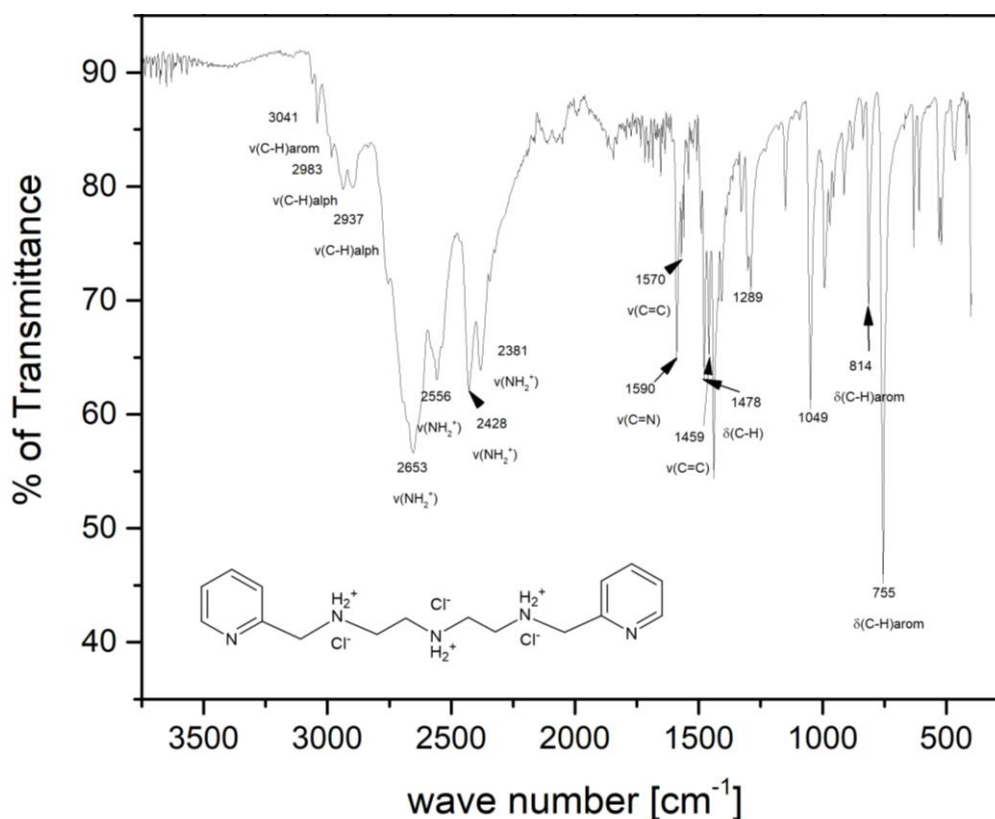


Fig. 12 IR spectrum of the $L^2 \cdot 3HCl$ compound.

5.2.3. NMR

5.2.3.1. ^1H Nuclear magnetic resonance of $\text{L}^2 \cdot 3\text{HCl}$

In the ^1H NMR at 400 MHz spectrum of the pentadentate ligand ($\text{L}^2 \cdot 3\text{HCl}$) dissolved in deuterated water (Fig.13) six signals corresponding to the different protons belonging to the molecule are identified. Four of these are considerably in a lower field in relation to the other 2. Between 7.51 and 8.52 ppm are found the signals corresponding to the aromatic protons of the pyridine rings H_1 - H_4 . The protons H_5 corresponding to the methylene groups of the alpha carbon of the pyridine rings are observed as a singlet between 4.3 and 4.38 ppm. Between 3.40 and 3.45 ppm a multiplet signal corresponding to 8 protons of the H_6 and H_7 hydrogens is observed.

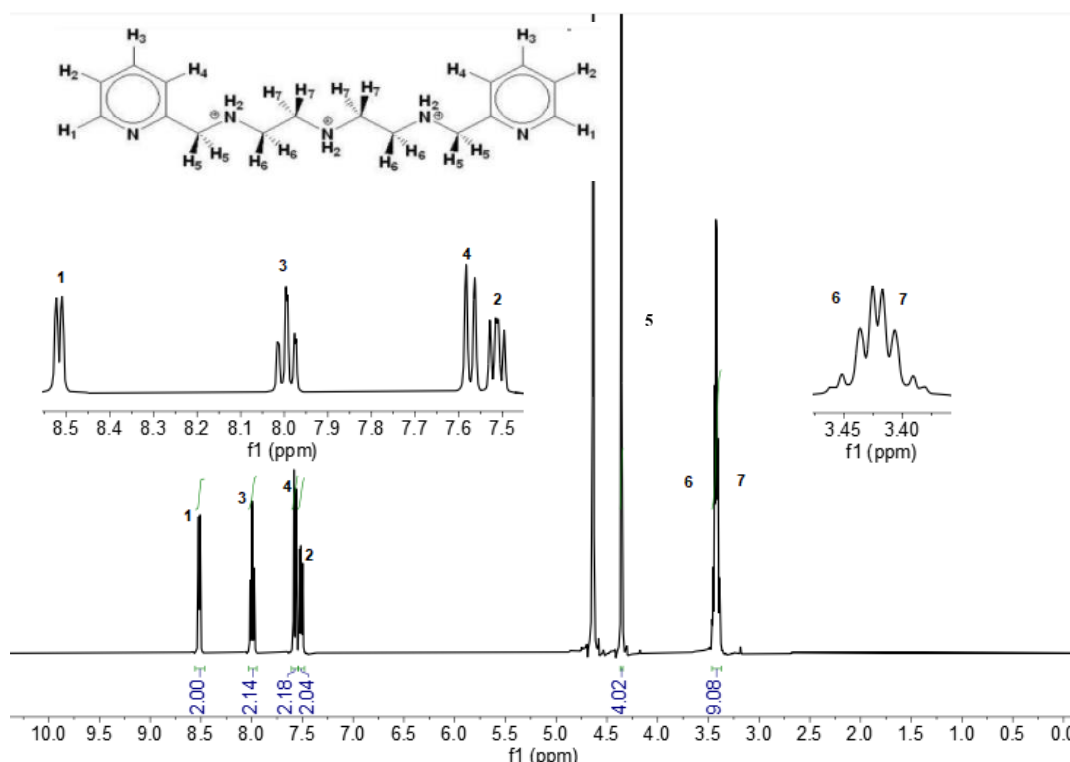


Fig. 13 ^1H NMR spectrum of the $\text{L}^2 \cdot 3\text{HCl}$ compound.

5.2.3.2. Coupling constants (J) of $\text{L}^2 \cdot 3\text{HCl}$.

As shown in Table. 3 hydrogen H_1 has three coupling constants with values of 5.3, 1.8 and 1.2 Hz, these correspond to the interaction with hydrogens H_2 , H_3 and H_4 shown in the inset of the Fig. 13, as the three hydrogens are not equivalents, these interactions would explain the ddd multiplicity. H_3 hydrogen has two coupling constants with values of 7.8 and 1.8 Hz corresponding to the interaction with H_4 and H_2 that at this system are considered equivalents,

and **H**₁, the interaction with this three hydrogens would explain the td multiplicity because the number of signal would be equal to (2+1)(1+1) = 6 for this hydrogen. Hydrogen **H**₄ has one coupling signal (7.8) Hz corresponding to the interaction with the hydrogen (**H**₃) this interaction would explain the d multiplicity obtained. Hydrogen **H**₂ has three coupling signals with values of (7.8, 5.3 and 1.2) Hz corresponding to the interaction with **H**₁, **H**₃ and **H**₄ hydrogens, in these case the three hydrogens are considered not equivalents, which would explain the *ddd* multiplicity as the number of signal would be equal to (1+1)(1+1)(1+1) = 8. The **H**₆ and **H**₇ hydrogens has one couplings with a value of (4.5) Hz this correspond to the interaction with each other, this explain the *t* multiplicity for this hydrogen. **H**₅ hydrogen does not shows signs of coupling with other hydrogens.

Table. 3 Summary of ¹H NMR data at 400MHz, in D₂O of compound L²•3HCl

δ (ppm)	Assignment	Multiplicity, integration	J(Hz)
8.52	H ₁	ddd,1H	J ₁₋₂ =5.3,J ₁₋₃ =1.8,J ₁₋₄ =1.2
7.51	H ₂	ddd,1H	J ₂₋₁ =5.3,J ₂₋₃ =7.8,J ₂₋₄ =1.2
8	H ₃	td,1H	J _{3-2,3-4} =7.8,J ₃₋₁ =1.8
7.57	H ₄	d,1H	J ₄₋₃ =7.8
4.36	H ₅	s,2H	-----
3.42	H ₆ -H ₇	t,4H	J ₆₋₇ =4.5

5.2.3.3. ¹³C Nuclear magnetic resonance of L²•3HCl

In the ¹³C NMR spectrum of the pentadentate ligand (L²) dissolved in deuterated water, (Fig. 14) 8 signals corresponding to the 8 different carbons present in the compound are observed. In the chemical shift range of $\delta = 149.66$ - 124.92 ppm, are found the signals belonging to **C**₁-**C**₅ carbons shown in the inset of the Fig. 14. The signal at $\delta = 50.43$ ppm corresponds to the methylene groups in α position to the pyridine rings, and the signals at $\delta = 44.17$ ppm and 43.17 ppm correspond to carbons **C**₈ and **C**₇, respectively.

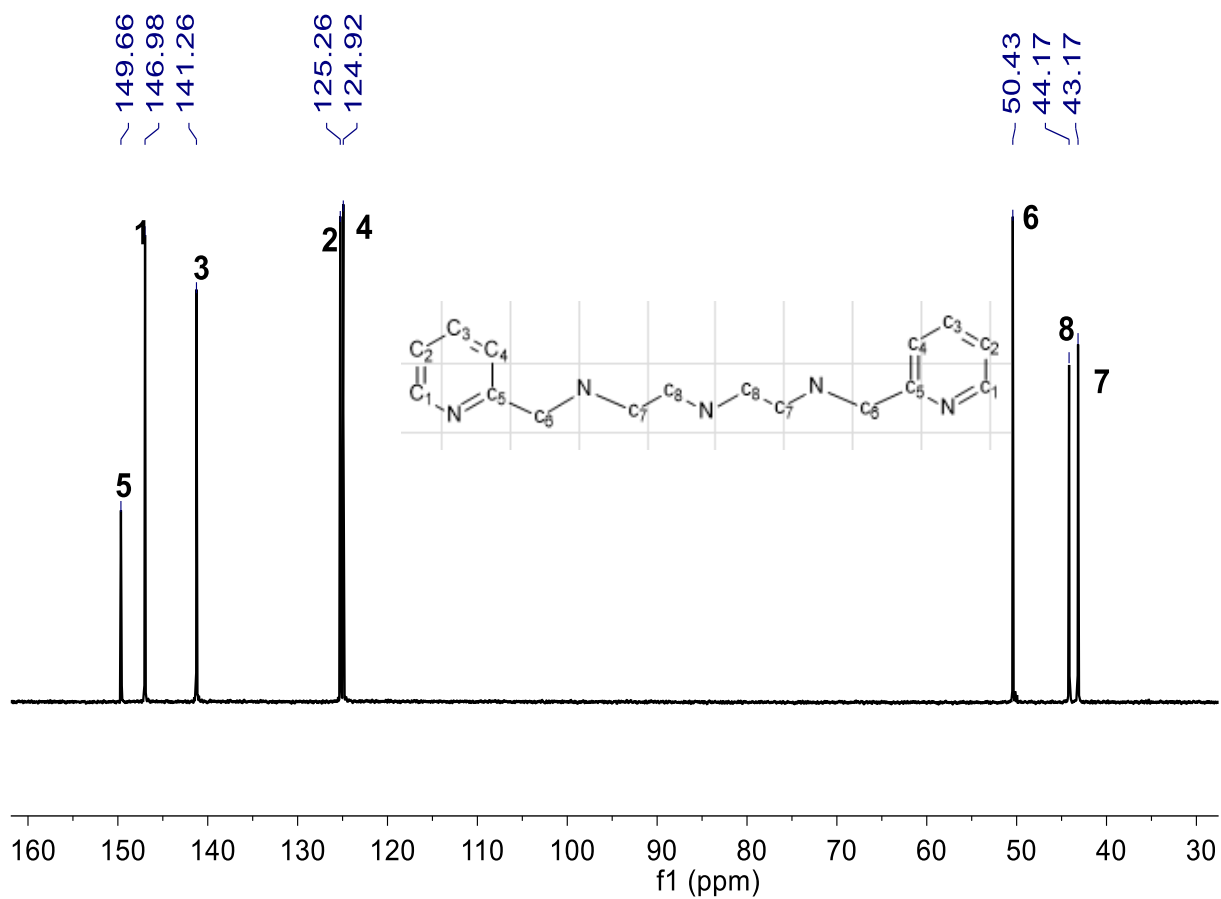


Fig. 14 ^{13}C NMR spectrum of the $\text{L}^2 \cdot 3\text{HCl}$ compound.

5.2.3.4. HSQC Spectrum for the $\text{L}^2 \cdot 3\text{HCl}$ compound

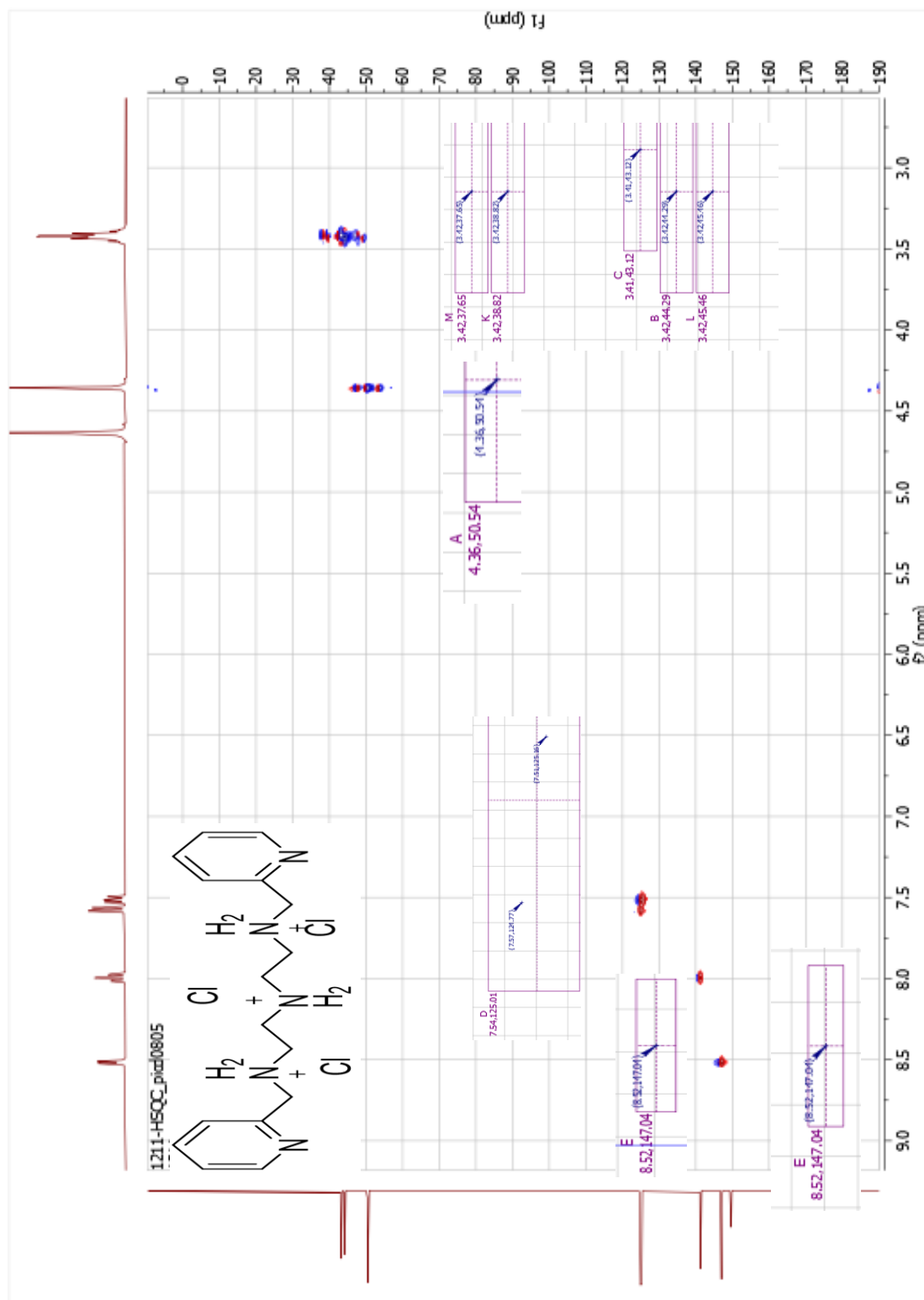


Fig. 15 HSQC spectrum of the $\text{L}^2 \cdot 3\text{HCl}$ compound.

The HSQC spectroscopy corroborate the assignment of the carbons and hydrogens made previously. The spectrum (Fig. 15) shows which hydrogens are directly attached to which carbon.

The hydrogen at $\delta = 8.52$ ppm (**H**₁) is coupled (attached) to the carbon at $\delta = 147.04$ ppm (**C**₁), very similar to the value of 146.98 ppm assigned to the carbon in the ¹³C NMR spectrum. The hydrogen at $\delta = 8$ ppm (**H**₃) is attached to the carbon at $\delta = 141.18$ ppm (**C**₃) value very similar to the one assigned 141.26 ppm. Hydrogens at $\delta = 7.57$ and 7.51 ppm (**H**₄ and **H**₂) are bound to carbons at $\delta = 124.92$ ppm (**C**₄) and $\delta = 125.26$ ppm (**C**₂). As expected, (**C**₅) carbon does not shows coupling to any hydrogen. The hydrogen signal in the HSQC spectrum at $\delta = 4.36$ ppm, corresponds to the signal at $\delta = 4.04$ ppm in the H NMR spectrum, which is bound to the carbon at $\delta = 50.43$ ppm (**C**₆). Finally, the hydrogens (**H**₆ and **H**₇) corresponding to the multiplet signal between $\delta = 3.40$ ppm and 3.45 ppm are attached to the carbon with $\delta = 43.17$ ppm (**C**₇) and 44.17 ppm (**C**₈).

5.2.4. Determination of the pKa values for L²•3HCl

Fig. 16 shows the titration curve obtained for the L²•3HCl ligand which was obtained using the methodology described in section 4.3.2.1.1. and was used to determine its pKa values.

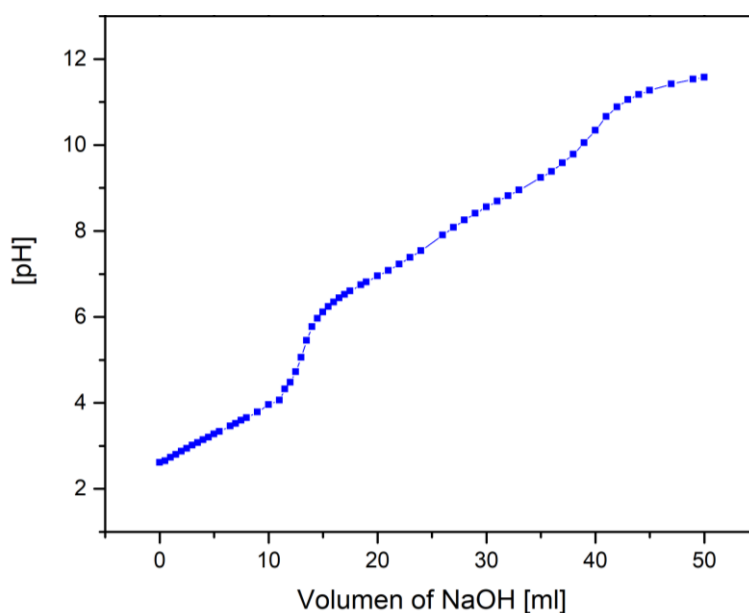
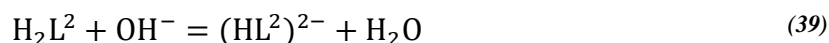
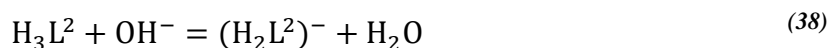


Fig. 16 titration curve for the L²•3HCl compound in aqueous medium.

We have an acid-base reaction for the L²•3HCl ligand of the form:





In Fig. 17 the first derivative for the titration curve for $L^2 \cdot 3HCl$ it is observed that the biggest changes in pH per volume of NaOH added are found at volumes of 13 mL, 25 mL and 40 mL.

The acidity constant for a weak acid in equilibrium can be expressed as:



In dilute solutions, can be expressed as a function of concentrations:

$$K_a = \frac{[A^-][H_3O^+]}{[HA]} \quad (42)$$

Applying decimal logarithms it is obtained that:

$$pH = pK_a + \log\left(\frac{[A^-]}{[HA]}\right) \quad (43)$$

In the first equivalence point the mol of OH^- equal the mol of acid $[H_3L^2]$ originally in the sample. So, at half the volume of the equivalence point the mol of the acid originally in the sample equals the mol of the first conjugated base $[H_2L^2]^-$. Then, for the first deprotonation eq. (38) the $pK_{a1} = pH$. Thus, for $L^2 \cdot 3HCl$ it is obtained a pK_{a1} equal to 3.46. At half the volume between the first and second equivalence point the $pK_{a2} = pH$, thus, for $L^2 \cdot 3HCl$ it is obtained a pK_{a2} equal to 6.81. Finally, at half the volume between the second and third equivalence point the $pK_{a3} = pH$. Thus, for $L^2 \cdot 3HCl$ it is obtained a pK_{a3} equal to 8.88.

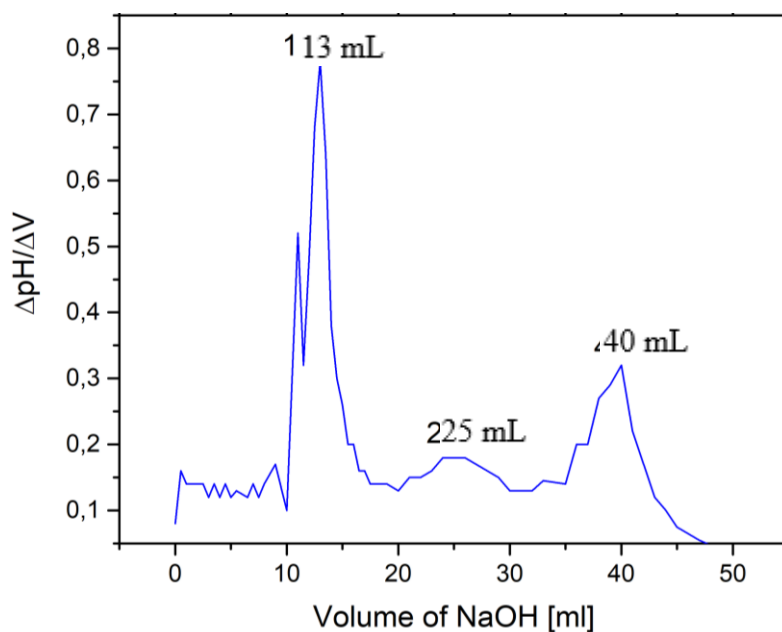


Fig. 17 First derivative of pH used for the pKa determination of the $L^2 \cdot 3HCl$ compound.

Data for the pKa calculation can be seen in the annexes, section 8.4. (Annexes).

5.3. 1,9-bis(3'pyridyl)-2,5,8- triazanoneno (L^3)

5.3.1. Synthesis of the trichlorohydrated $L^3 \cdot 3HCl$

The synthesis of the trichlorohydrated $L^3 \cdot 3HCl$ was performed following the next reaction scheme:

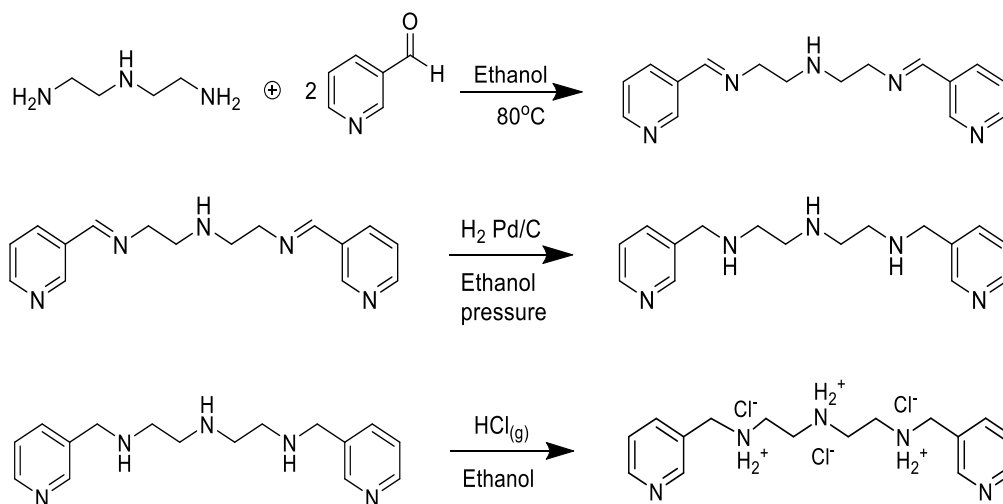


Fig. 18 General scheme of the synthesis of the trichlorohydrate L^3 compound.

5.3.2. Elemental analysis of the $L^3 \cdot 3HCl$ ligand

The percentage of carbon, hydrogen and nitrogen present in the $L^3 \cdot 3HCl$ ligand was determined. Table. 4 shows the experimental results obtained, these, agree with the theoretical data calculated for the percentage of each atom contained in the ligand. As it can be seen the experimental results shows the presence of sulfur in the sample, although quite small (0.009%), this was assigned to sample contamination.

Table. 4 Experimental and theoretical elementary analysis of $L^3 \cdot HCl$ compound.

Element	Experimental	Theoretical
C	47,612% \pm 0,081%	48,679 %
H	6,619 % \pm 0,065%	6,638 %
N	17,313% \pm 0,211%	17,740 %
S	0,009% \pm 0,062%	-----
Cl	-----	26,942 %

5.3.3. Infrared spectrum of the $L^3 \cdot 3HCl$ compound

The C-H vibration of alkanes is found at 3000 cm^{-1} . The sp^3 C-H absorption, always occurs at frequencies less than 3000 cm^{-1} ($3000\text{-}2840 \text{ cm}^{-1}$). Thus, in the infrared spectrum (Fig. 19) one can observe the bands for $\nu(\text{C-H})$ vibrations from the aliphatic part of the compound (L^3) at 2982 and 2928 cm^{-1} . The vibrations corresponding to the $\nu(\text{N-H}_2^+)$ bonds of the protonated amines in the aliphatic chain are found at 2663 , 2552 , 2427 and 2384 cm^{-1} . Two bands are observed at 1577 y 1451 cm^{-1} for the $\nu(\text{C=C})$ vibration of the pyridine rings. At 1478 cm^{-1} is observed the band corresponding to the $\delta(\text{C-H})$ of the methylenes present in the aliphatic part of the compound. $\delta(\text{C-H})$ oop bending are present at 800 and 717 cm^{-1} resulting from strong coupling with adjacent hydrogens atoms for the monosubstitution pattern.

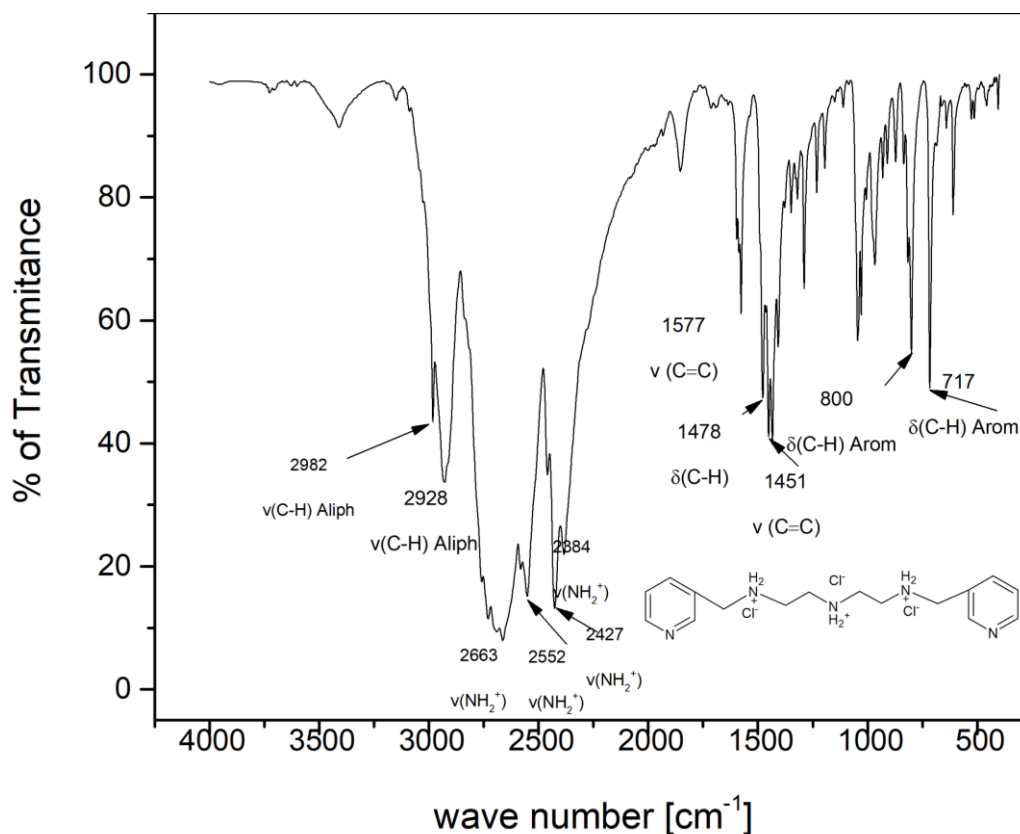


Fig. 19 IR spectrum of the $L^3 \cdot 3HCl$ compound.

5.3.4. NMR

5.3.4.1. 1H Nuclear magnetic resonance of $L^3 \cdot 3HCl$

In the 1H NMR at 400 MHz spectrum of the pentadentate ligand ($L^3 \cdot HCl$) dissolved in deuterated water (Fig. 20) six signals corresponding to the different protons belonging to the molecule are identified. Four of these are considerably in a lower field in relation to the other 2. Between $\delta = 8.5$ and 7.4 ppm are found the signals corresponding to the aromatic protons of the pyridine rings H_1 - H_4 shown in the inset of the Fig. 20. The protons H_5 corresponding to the methylene groups of the alpha carbon of the pyridine rings are observed as a singlet at $\delta = 4.3$ ppm. Between $\delta = 3.25$ and 3.45 ppm a multiplet signal corresponding to 8 protons of the H_6 and H_7 hydrogens is observed.

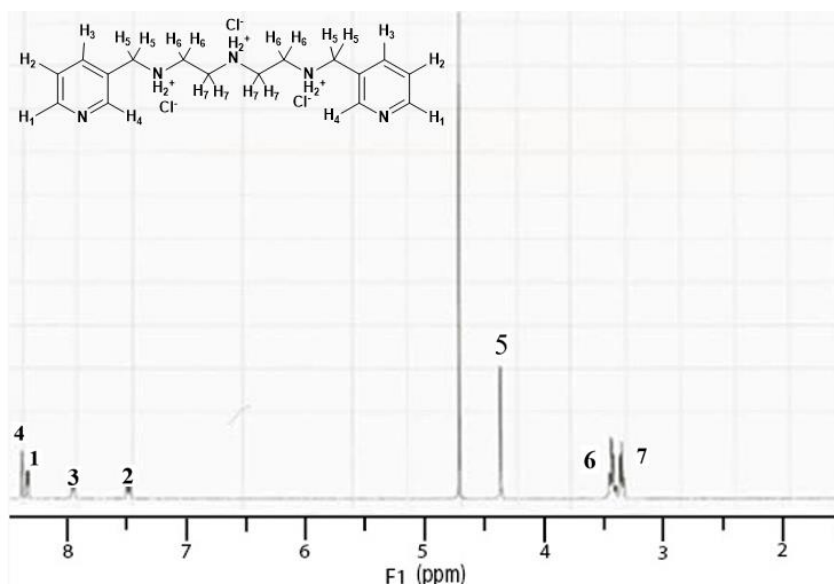


Fig. 20 ^1H NMR spectrum of the $\text{L}^3\cdot 3\text{HCl}$ compound.

5.3.5. Determination of the pKa values for $\text{L}^3\cdot 3\text{HCl}$

Fig. 21 shows the titration curve obtained for the $\text{L}^3\cdot 3\text{HCl}$ ligand which was obtained using the methodology described in section (4.3.3.1.1.) and was used to determine its pKa values.

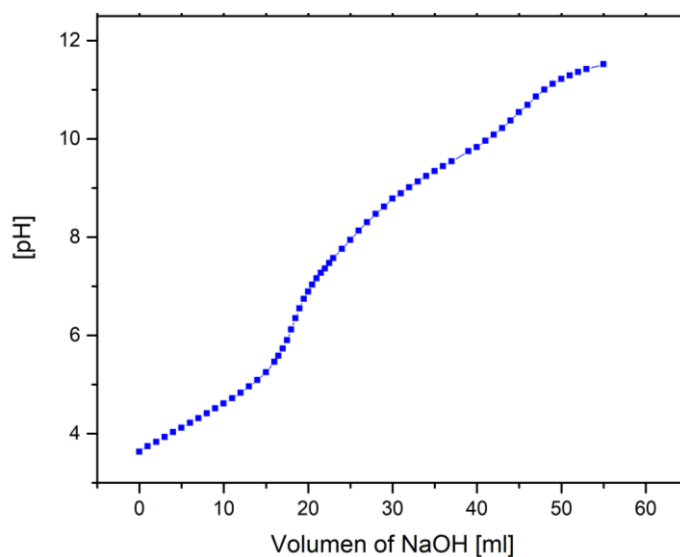
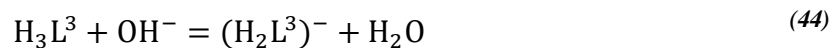
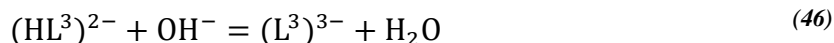
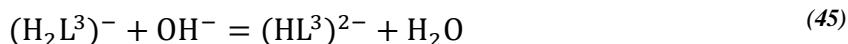


Fig. 21 titration curve for the $\text{L}^3\cdot 3\text{HCl}$ compound in aqueous medium.

For this ligand it is obtained an acid-base reaction of the form:





In Fig. 22 the first derivative for the titration curve for $\text{L}^3\cdot 3\text{HCl}$ is presented and the calculation of their pK_a was obtained as described for the $\text{L}^2\cdot 3\text{HCl}$ ligand. It is observed that the biggest change in pH per volume of NaOH added are found at a volume of 18 mL (first equivalence point). At half the volume of this first equivalence point for the first deprotonation, the $\text{pK}_{a1} = \text{pH}$. Thus, for $\text{L}^3\cdot 3\text{HCl}$ it is obtained a pK_{a1} equal to 4.51. For this ligand the peaks for the second and third equivalence points were very hard to obtain graphically so those pK_a were obtained mathematically. At half the volume between the first and second equivalence point the $\text{pK}_{a2} = \text{pH}$, thus, for $\text{L}^3\cdot 3\text{HCl}$ it is obtained a pK_{a2} equal to 7.57. Finally, at half the volume between the second and third equivalence point the $\text{pK}_{a3} = \text{pH}$. Thus, for $\text{L}^3\cdot 3\text{HCl}$ is obtained and had a value of 9.44.

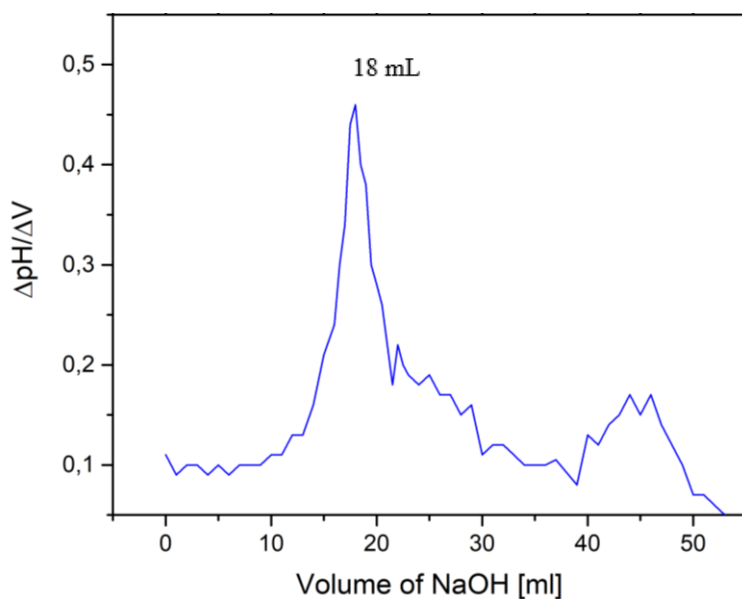


Fig. 22 First derivative of pH used for the pK_a determination of the $\text{L}^3\cdot 3\text{HCl}$ compound.

Table 5 shows the pK_a values obtained for the $\text{L}^2\cdot 3\text{HCl}$ and $\text{L}^3\cdot 3\text{HCl}$ compounds.

Table. 5 pK_a comparison between $\text{L}^2\cdot 3\text{HCl}$ and $\text{L}^3\cdot 3\text{HCl}$.

$\text{L}^2\cdot 3\text{HCl}$

$\text{L}^3\cdot 3\text{HCl}$

V_{eq1} [mL]	6.5	9
pK_{a1}	3.46	4.51
V_{eq2} [mL]	19	23
pK_{a2}	6.81	7.57
V_{eq3} [mL]	32.5	44
pK_{a3}	8.88	9.44

As shown in Table. 5, the pK_a values for the $L^2 \cdot 3HCl$ ligand in aqueous medium are lower than those obtained for the $L^3 \cdot 3HCl$. Therefore, it can be said that it is easier to lose hydrogens for the pentaamine ligand that has the pyridine ring substitution at position 2, than for its counterpart at position 3. This factor could be decisive for the dehydrogenation reaction to occur.

5.4. Kinetics

5.4.1. Rate constant calculation for the reaction between L^2 and



After mixing equimolar amounts of compound $[Fe(DMSO)_6]^{3+}(NO_3)_3$ with the L^2 ligand, the kinetics of the oxidative dehydrogenation reaction were followed by UV-Vis spectrophotometry in a range of 700 to 190 nm for 450 minutes (Fig. 23). During the time in which the reaction was carried out, two peaks were observed one around 200 nm corresponding to a charge transfer, and another at 258 nm assigned to the reaction progress. It was observed that as it progressed, the absorbance at its peak at 258 nm decreased.

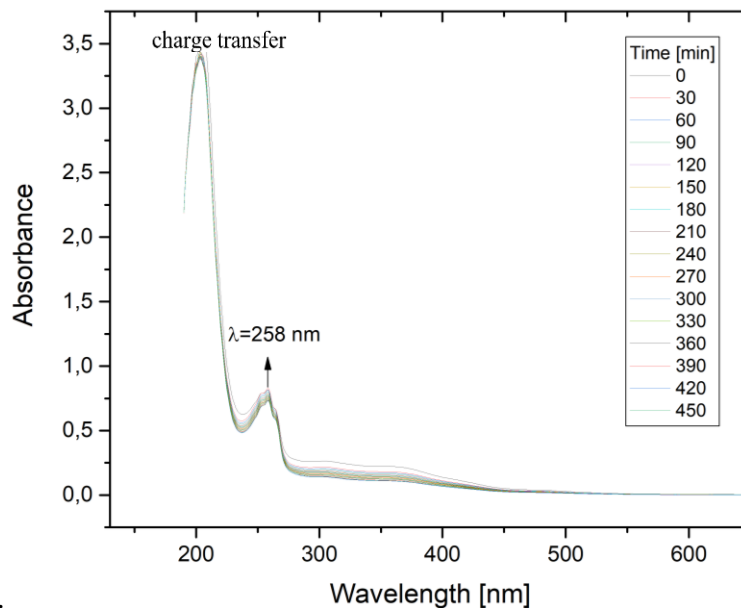


Fig. 23 UV-Vis spectrum with respect to time, between L^2 and $[\text{Fe}(\text{DMSO})_6](\text{NO}_3)_3$

Explanation for the rate constant calculation show below were taken from²⁴:

In a reaction $A \rightarrow B$ in which a property P (in our case the absorbance), is followed through time and depends on the reactant and the products, if p_A and p_B represent the proportionality constants between concentration and property, and C is a constant contribution then the value P at any time t is given by:

$$P_t = p_A[A] + p_B[B] + C \quad (47)$$

Substitution of the first order equation gives:

$$P_t = p_A[A]_0 \exp(-kt) + p_B[A]_0 [1 - \exp(-kt)] + C \quad (48)$$

The initial and final instruments readings are:

$$P_0 = p_A[A]_0 + C \quad (49)$$

$$P_\infty = p_B[A]_0 + C \quad (50)$$

Substitution of those equations in Eq. (48) yields upon rearrangement,

$$\frac{P_t - P_\infty}{P_0 - P_\infty} = \exp(-kt) \quad (51)$$

$$\ln(P_t - P_\infty) - \ln(P_0 - P_\infty) = -kt \quad (52)$$

$$\ln(P_t - P_\infty) = -kt + \ln(P_0 - P_\infty) \quad (53)$$

Thus a plot of $\ln(P_t - P_\infty)$, or $\ln(P_\infty - P_t)$ if the values of P increase with time so that the natural logarithm is always positive, against time is a straight line of slope $-k$.

Fig. 24 shows the relationship between absorbance and time, as mentioned, it decreases as the reaction progresses.

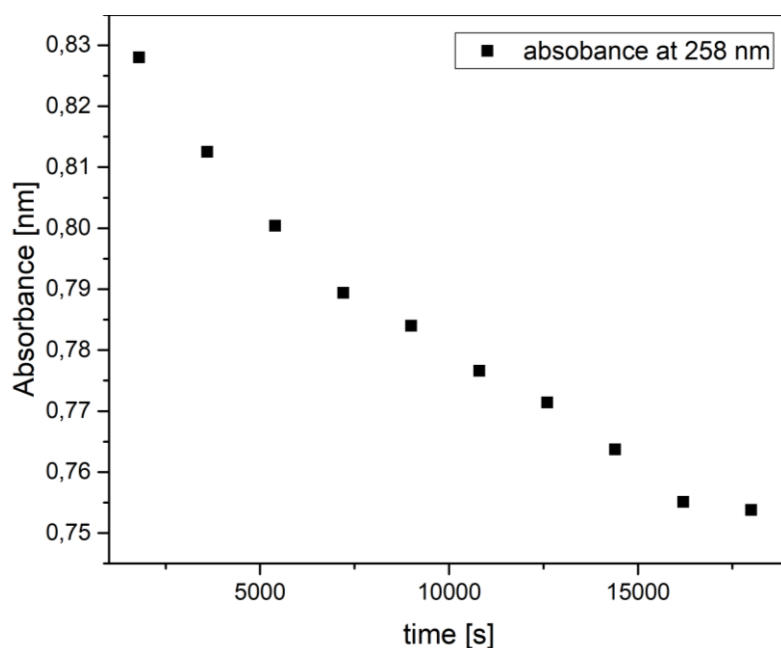


Fig. 24 Plot of absorbance vs time for the reaction between L^2 and $[\text{Fe}(\text{DMSO})_6](\text{NO}_3)_3$ taken at the peak of maximum absorbance seen at 258 nm.

5.4.2. Kezdy-Swinbourne treatment

Sometimes, the final instrument reading P_∞ (in this case the absorbance at time $t = \infty$) is unreliable or unavailable. In certain cases, especially when the reaction follows first order kinetics, the data can be treated satisfactorily without knowing this value.²³

Consider first order kinetic data at time t and at time Δt later, the value of P at each time is:

$$P_t = (P_0 - P_\infty) \exp(-kt) + P_\infty \quad (54)$$

$$P_{t+\Delta t} = (P_0 - P_\infty) \exp[-k(t + \Delta t)] + P_\infty \quad (55)$$

Here two spaced values are divided;

$$\frac{P_t - P_\infty}{P_{t+\Delta t} - P_\infty} = \exp(k\Delta t) \quad (56)$$

Solving for P_t we have:

$$P_t = P_\infty [\exp(k\Delta t) - 1] + P_{t+\Delta t} \exp(k\Delta t) \quad (57)$$

The first term on the right is time independent. From eq. (57) it is obtained that for a first order reaction a plot of P_t vs $P_{t+\Delta t}$ will be linear with a slope of $\exp(k\Delta t)$. The rate constant is then calculated from the slope by using the value of Δt chosen, originally dividing the data set into two parts.

Since at the end point $P_t = P_{t+\Delta t} = P_\infty$, the intersection of the linear fit of the absorbance at time t vs the absorbance at time $t + \Delta t$ with a 45° line (with equation $y = x$) gives the value of P_∞ .

The Kezdy-Swinbourne plot must be linear, with an experimental error, if the reaction follows a first order kinetics. Although, the linearity of these plots, unlike the plot of $\ln(P_t - P_\infty)$ against time, does not constitute proof of first order kinetics.

So, for the kinetic reaction followed by UV-Vis spectroscopy between L^2 and $[\text{Fe}(\text{DMSO})_6](\text{NO}_3)_3$ and according to eq. (57) it is obtained the next plot:

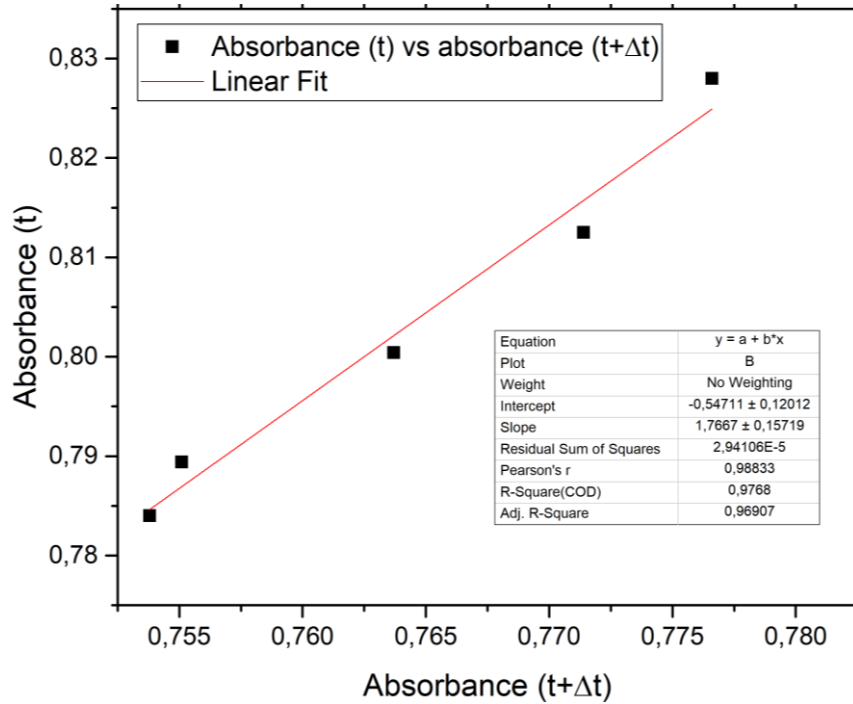


Fig. 25 Linear fit of the absorbance (t+Δt) vs absorbance (t) for the rate constant determination for the reaction between L^2 and $[Fe(DMSO)_6](NO_3)_3$.

From Fig. 25 and eq. 57 the following information for a first order kinetic is obtained:

$$slope = exp(k\Delta t) \quad (58)$$

$$1.7667 = exp(k\Delta t) \quad (59)$$

$$\ln(1.7667) = k * \Delta t \quad (60)$$

$$k = \frac{\ln(1.7667)}{10800 \text{ s}} \quad (61)$$

$$k = 5.269 * 10^{-5} \text{ s}^{-1} \quad (62)$$

The absorbance at $t = \infty$ (A_∞) is calculated from the interception of the linear fit equation between Absorbance ($t + \Delta t$) vs Absorbance at t and the line of 45° that is the line with equation $y = x$.

So we have two equations for this measurement:

$$y = 1.7667x - 0.5471 \quad (63)$$

$$y = x \quad (64)$$

Replacing eq. (64) in eq. (63) it is obtained that:

$$y = 0.7667y - 0.5471 \quad (65)$$

$$y = A_{\infty} = 0.714 \quad (66)$$

Then according to eq. 66 $A_{\infty} = 0.714$

As mentioned before, the linearity of the plot of $\ln(P_t - P_{\infty})$ vs t with this case been P the absorbance (Fig. 26) is a proof of a first order kinetic reaction. And we can see in Fig. 26 that this plot give us a value of R square of 0.9912 for the adjustment of the values with a linear plot.

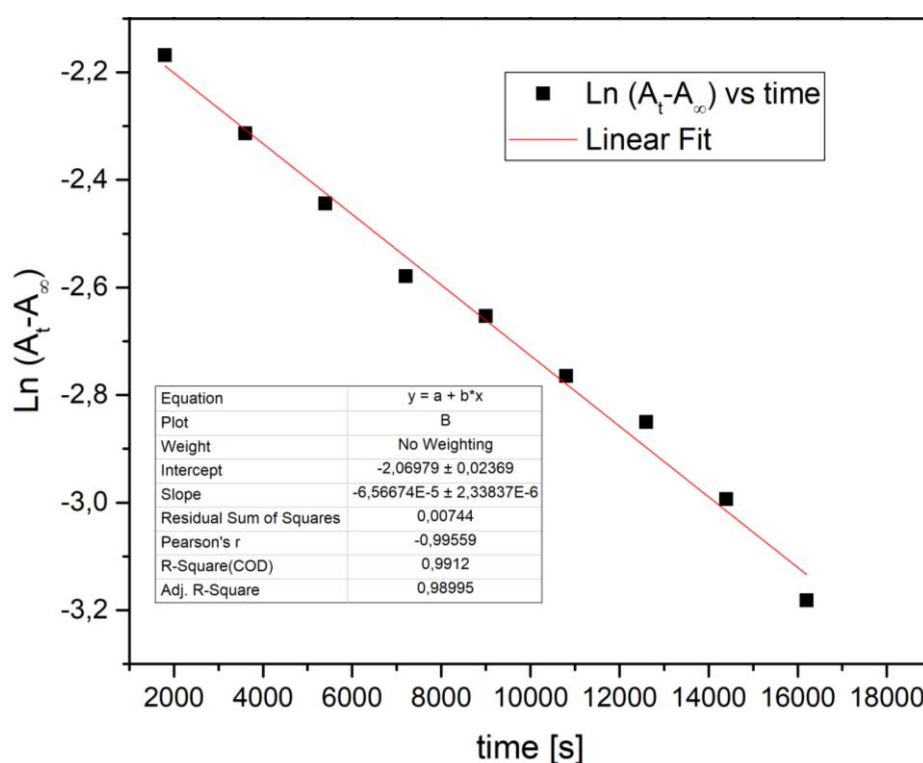


Fig. 26 Linear fit of the $\ln(A_t - A_{\infty})$ vs time (t) plot used as proof for the presence of a first order kinetic reaction between L^2 and $[\text{Fe}(\text{DMSO})_6](\text{NO}_3)_3$.

The UV-Vis spectrum of the $[\text{Fe}^{\text{II}}L^4]^{2+}$ complex synthesis reaction at a concentration of 0.015 M (Fig. 27) allowed us to observe two absorbance bands corresponding to transitions in the range of the visible (576 nm) and ultraviolet (382 nm) spectrum. This result shows the change

in the electronic state of iron, because, electronic transitions between the t_{2g} and e_g molecular orbitals causing the presence of the absorbance bands in the spectra are prohibited by spin and by Laporte for the Fe^{3+} (d^5) of HS^{24} . The appearance of the two absorbance peaks suggests a change in the oxidation state of the transition metal from +3 to +2. According to the Tanabe Sugano diagram Section 8.5. (Annexes) for a d^6 LS specie, 5 transitions are allowed (${}^1A_1 \rightarrow {}^1T_1$; ${}^1A_1 \rightarrow {}^1T_2$, ${}^1A_1 \rightarrow {}^1E$, ${}^1A_1 \rightarrow {}^1E_1$, ${}^1A_1 \rightarrow {}^1A_2$) and for a d^6 HS specie 1 transition (${}^5T_2 \rightarrow {}^5E$). This suggests for the final complex a diamagnetic d^6 low spin species in which the rest of the transitions are hidden in the UV range.

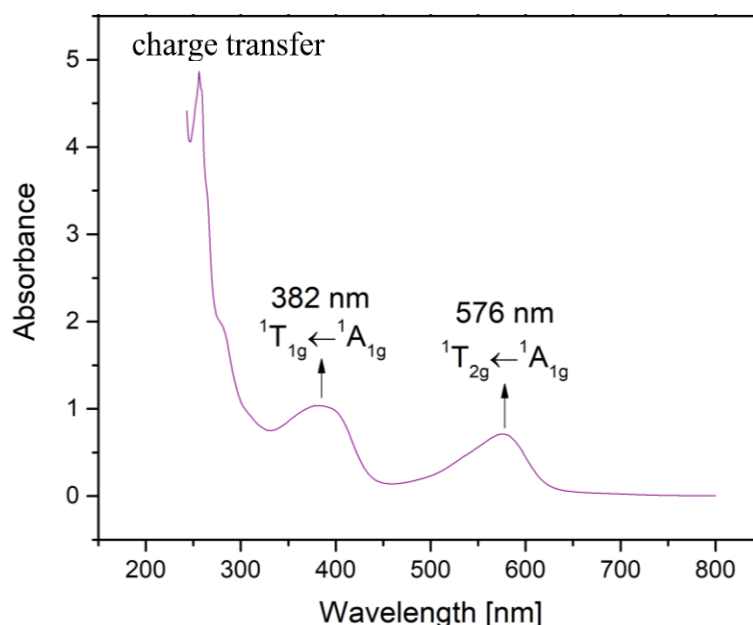


Fig. 27 UV-vis absorbance spectra of the $[\text{Fe}^2\text{L}^4]^{2+}$ compound at a 0.015M concentration.

5.4.3. UV-Vis spectrum in aqueous solution and diffuse reflectance for the $[\text{Fe}(\text{DMSO})_6](\text{NO}_3)_3$ complex.

As observed in section 5.1.1., for the result of the magnetic moment of the compound $[\text{Fe}(\text{DMSO})_6](\text{NO}_3)_3$, a value of 5.73 BM was obtained, which led us to conclude that we are in the presence of a HS Fe (III) specie²². In both, the UV-Vis spectrum carried out in aqueous solution and the diffuse reflectance UV-Vis spectra (Fig. 28), the transitions in the visible are not observed, confirming the 3+ oxidation state and the electronic state of Fe^{3+} since, in the Tanabe Sugano diagram for this specie (Section 8.4.) there are not allowed transitions by spin and Laporte expected because its basal state is a ${}^6A_{1g}$, also one cannot find any excited state with this multiplicity.

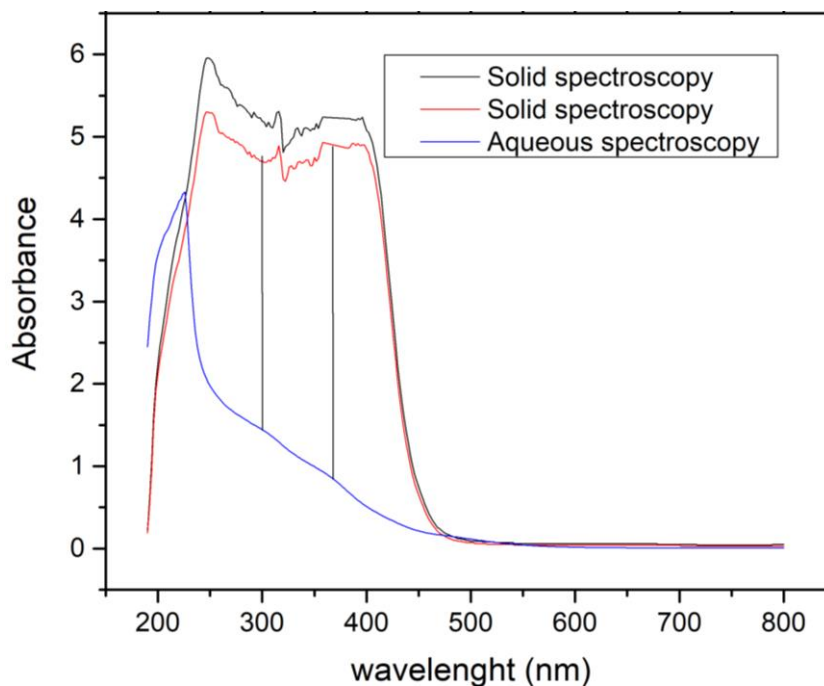


Fig. 28 Comparison between liquid and solid (diffuse reflectance) UV-Vis absorbance of $[\text{Fe}(\text{DMSO})_6](\text{NO}_3)_3$.

When comparing the spectra given by UV-Vis (in aqueous solution) and DRS-UV-Vis (for solids), it is observed that the absorbance peaks coincide for both spectra. This indicates that the coordination sphere of $[\text{Fe}(\text{DMSO})_6]^{3+}$ is not affected (substituted) by the H_2O molecules at the time of adding the Iron complex in the aqueous medium.

5.4.4. Calculation of the rate constant for the reaction between L^3 and $[\text{Fe}(\text{DMSO})_6]^{3+}(\text{NO}_3)_3$

After mixing equimolar amounts of compound $[\text{Fe}(\text{DMSO})_6]^{3+}(\text{NO}_3)_3$ with the L^3 ligand, the kinetics of the oxidative dehydrogenation reaction were followed by UV spectrophotometry in a range of 800 to 190 nm for 330 minutes (Fig.29).

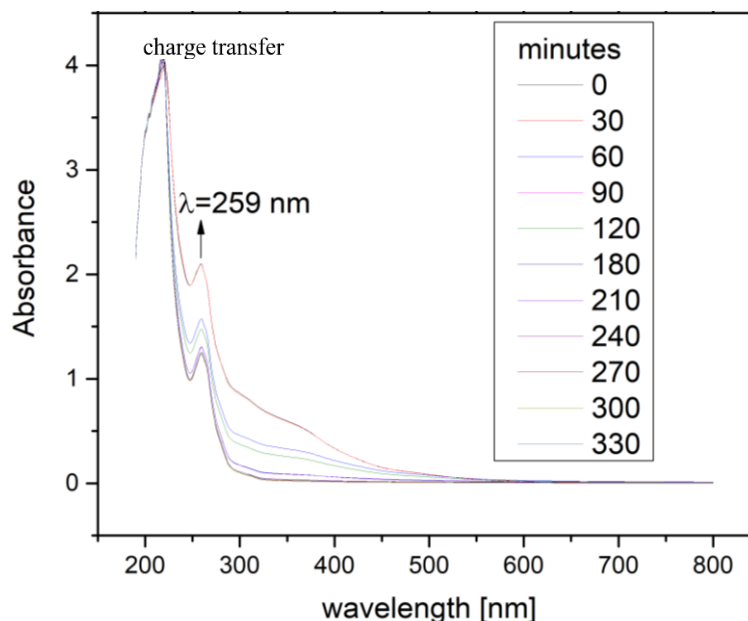


Fig. 29 UV-Vis spectra for the reaction between L^3 and $[Fe(DMSO)_6](NO_3)_3$

The spectral changes in absorbance observed as the reaction progresses, Fig. 29 shows an offspring of the absorbance measured at the maximum peak observed at 259 nm for the reaction between the L^3 ligand and the $[Fe(DMSO)_6](NO_3)_3$.

For this reaction, even with the changes in the concentration of the reagents, it was not possible to observe the formation of the absorption bands observed for the reaction with L^2 , even more, almost instantaneous precipitation of a compound was observed. This suggests that the oxidation state of the iron did not change during the reaction and as mentioned before this is necessary for the OD to occur, therefore, such reaction does not occur for the system with the L^3 ligand. This could be influenced by the high pKa values obtained for this ligand ($pK_{a1} = 4.51$; $pK_{a2} = 7.57$; $pK_{a3} = 9.44$) compared to its counterpart with the substitution in the position 2 of the pyridine rings ($pK_{a1} = 3.46$; $pK_{a2} = 6.81$; $pK_{a3} = 8.88$). As it has been seen¹³, the loss and transfer of hydrogen from the ligand to the metal influences the intramolecular transfer of electrons between the ligand, the metal and with oxygen so that oxidative dehydrogenation occurs.

In the Figures below, (Fig. 30) one can see the results obtained for this reaction. The calculations made to obtain the rate constant for this system are based on this plot and are presented as well.

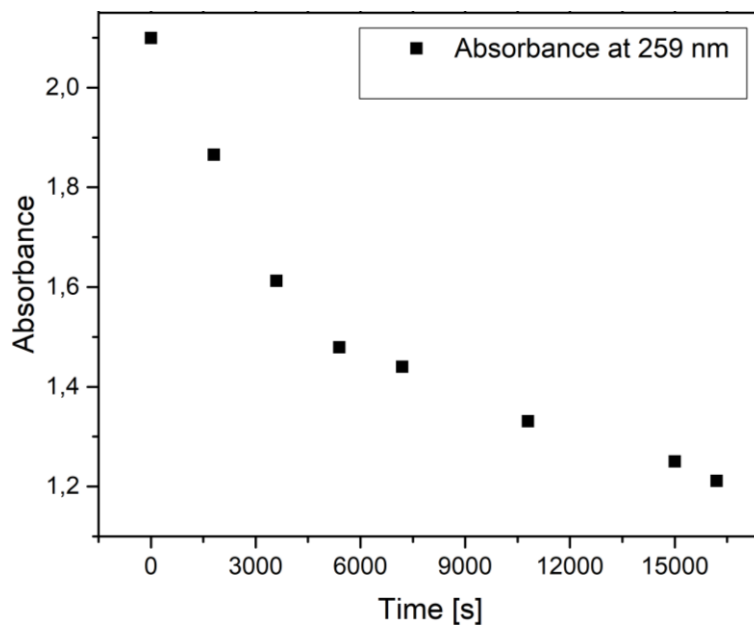


Fig. 30 Absorbance vs time for the reaction between L^3 and $[Fe(DMSO)_6](NO_3)_3$ taken at the peak of maximum absorbance seen at 259 nm.

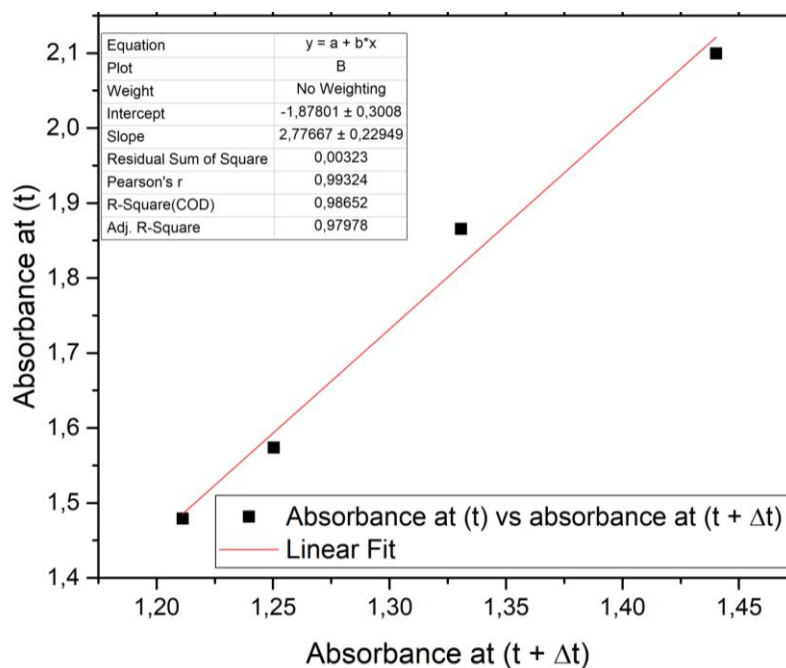


Fig. 31 Linear fit of the absorbance (t+Δt) vs absorbance (t) for the rate constant determination for the reaction between L^3 and $[Fe(DMSO)_6](NO_3)_3$.

As well as before, from Fig. 31 the rate constant for the reaction with the L³ ligand it is obtained:

$$k = \frac{\ln(2.7767)}{7200 \text{ s}} = 1.4184 * 10^{-4} \text{ s}^{-1} \quad (67)$$

The infinite absorbance (A_{∞}) is calculated from the interception of the linear fit between the absorbance ($t + \Delta t$) vs absorbance at t and the line at 45° that is the line with the equation $y = x$. As before, the A_{∞} was determined using the same methodology as for the reaction with the L² ligand giving that:

$$y = A_{\infty} = 1.057 \quad (68)$$

As mentioned before, the linearity of the plot of $\ln(P_t - P_{\infty})$ vs t , with P for this case been the absorbance, is a proof of a first order kinetic reaction. And we can see in Fig. 32 that this plot give us a value of R square of 0.974 for the adjustment of the values with a linear plot.

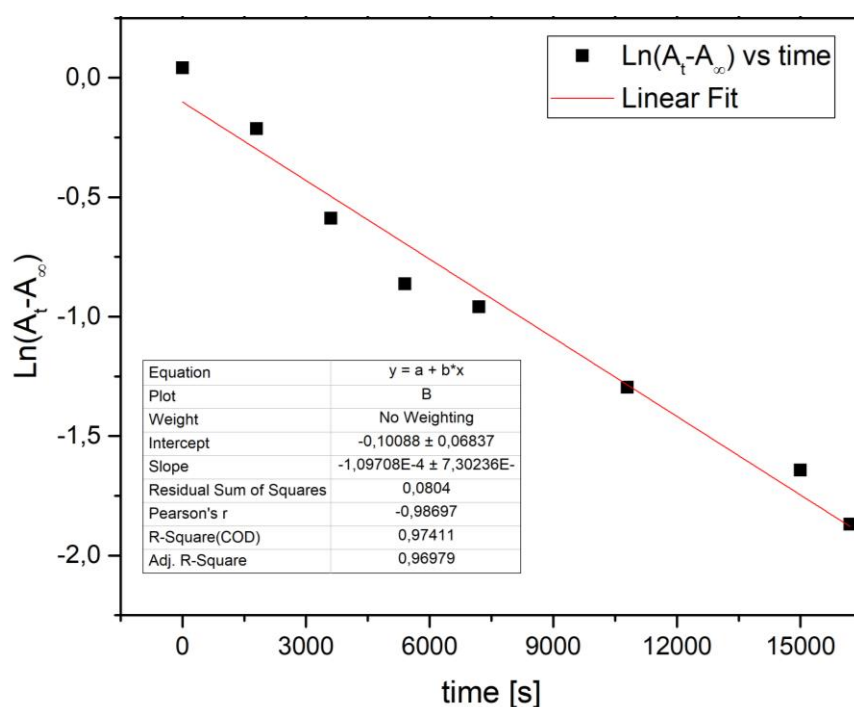


Fig. 32 Linear fit of the $\ln(A_t - A_{\infty})$ vs time (t) plot used as proof for the presence of a first order kinetic reaction between L³ and $[\text{Fe}(\text{DMSO})_6](\text{NO}_3)_3$.

Table. 6 shows the rate constants for the reaction between the L² and L³ ligands with the $[\text{Fe}(\text{DMSO})_6](\text{NO}_3)_3$ complex.

Table. 6 Comparison of the rate constants obtained for the reaction between L² and L³ with [Fe(DMSO)₆](NO₃)₃

	k [s ⁻¹]
[Fe(II)L ⁴] ²⁺	5.269 * 10 ⁻⁵ s ⁻¹
[Fe(III)L ³] ³⁺	1.4184 * 10 ⁻⁴ s ⁻¹

Table. 6 shows that the rate constant for the reaction between L³ and L² ligand with the [Fe(DMSO)₆](NO₃)₃ complex is of a different magnitude than for the similar reaction with L². Studies of OD reactions for an hexadentate ligand in ethanolic medium under oxygen atmosphere²⁸, divided the reaction into two main steps, first, the coordination of the hexadentate ligand to the transition metal, and second the oxidative dehydrogenation process. In the study, the two mentioned steps were observed by monitoring the reaction by UV-Vis spectrophotometry. Therefore, it was possible to determine the rate constants for both reaction steps. Constants (k_{obs}) were always found with bigger order of magnitude for the coordination step of the ligand to the metal center, indicating that this occurs much faster than oxidative dehydrogenation²⁵. It was found through the rate constant for both reactions that the one in which oxidative dehydrogenation did not occur has a bigger value, which is consistent with previous studies. Therefore, although the two steps of the reaction could not be observed using the UV-Vis spectra information, the constant values obtained for the reaction in which the oxidizing-reductive process occurs, might suggest that is influenced by the OD step.

5.5. Cyclic voltammetry

5.5.1. Cyclic voltammetry for the [Fe(DMSO)₆](NO₃)₃ complex in aqueous medium

The voltamperogram (Fig. 33) was obtained starting from the potential of zero current and starting the scan in a positive direction. An oxidation signal is observed with an anodic peak potential E_a = 0.7086 V / Ag-AgCl. When the scan is reversed, a reduction signal is observed with a cathodic peak E_c = 0.3326 V/Ag-AgCl. The E_{1/2} value for this system is 0.5206 V / Ag-AgCl.

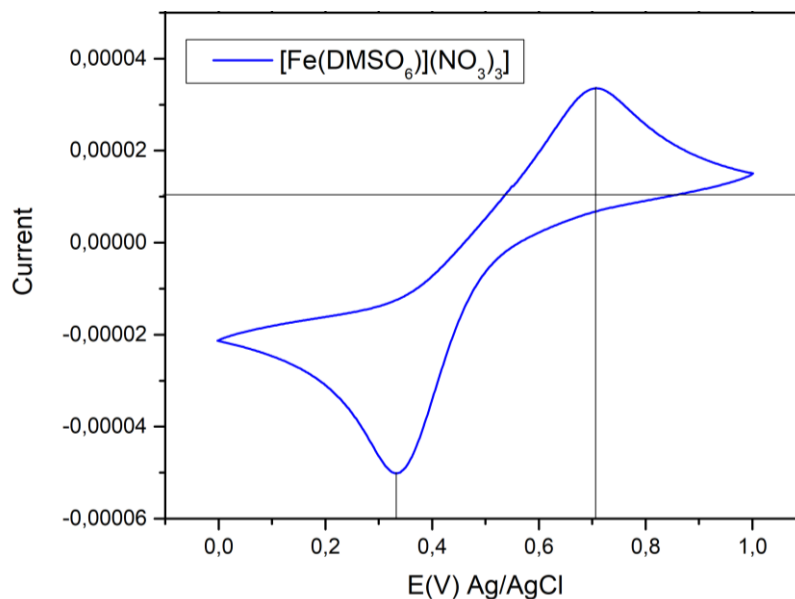


Fig. 33 CV for the $[\text{Fe}(\text{DMSO})_6](\text{NO}_3)_3$ compound, both vertical lines indicate the anodic and cathodic potentials obtained under the conditions of study.

These values are attributed to the oxidation and reduction of the transition metal (Fe) in the system. Therefore, the electrochemical species (Fe) present in the solution undergoes an electrochemical reaction that can be represented as follows:



5.5.2. Cyclic voltammetry for the $[\text{Fe(II)}\text{L}^4]^{2+}$ complex in aqueous medium

In Fig. 34 a comparison is made between the CV spectra between the $[\text{Fe}(\text{DMSO})_6](\text{NO}_3)_3$ and $[\text{Fe(II)}\text{L}^4]^{2+}$ compounds. The voltamperograms were obtained starting from the potential of zero current and initiating the scanning in a positive direction. For the $[\text{Fe}(\text{DMSO})_6](\text{NO}_3)_3$ complex (black spectrum), unlike the $[\text{Fe(II)}\text{L}^4]^{2+}$ complex (red spectrum), two pairs of redox potentials are observed, these are associated with the oxidation and reduction of both the transition metal and the coordinated ligand, a characteristic process of the oxidative dehydrogenation reaction. The peak of anodic potential corresponding to the oxidation for iron is $E_a(\text{Fe}) = 0.723 \text{ V/Ag-Ag-Cl}$ and that of reduction $E_c(\text{Fe}) = 0.1588 \text{ V/Ag-Ag-Cl}$. The $E_{1/2}$ value for this system is $0.4409 \text{ V/Ag-Ag-Cl}$.

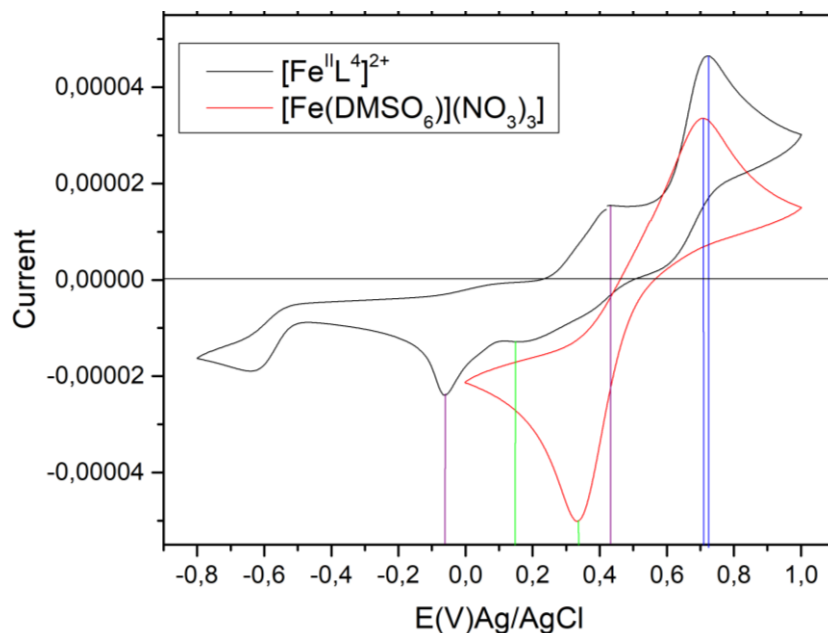


Fig. 34 Comparison between the CV for the $[\text{Fe(II)L}^4]^{2+}$ and $[\text{Fe(DMSO)}_6](\text{NO}_3)_3$ compounds, vertical lines indicate the anodic and cathodic potentials obtained under the conditions of study.

The new redox pair which corresponds to the oxidation and the reduction of the ligand, has an oxidation potential $E_a(\text{L}^2) = 0.432 \text{ V / Ag-Ag-Cl}$ and reduction $E_c(\text{L}^2) = -0.06 \text{ V/Ag-Ag-Cl}$. The value of $E_{1/2}$ for this system is 0.186 V/Ag-Ag-Cl . The mean value for the redox state associated with Fe does not coincide with that of $[\text{Fe(DMSO)}_6](\text{NO}_3)_3$ this can be attributed to the change in the coordination sphere from the reaction with the L^3 to the reaction with the L^2 ligand.

The ligand oxidation is a process that requires the transfer of two electrons and protons, which can be expressed in the following equation:



5.5.3. Cyclic voltammetry for the $[\text{Fe(III)L}^3]^{3+}$ complex in aqueous medium

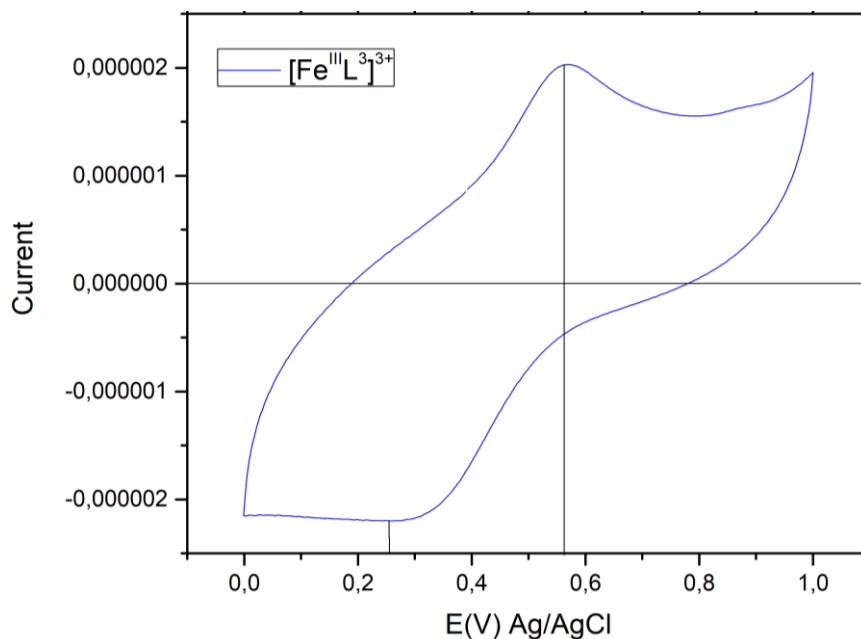


Fig. 35 CV for the $[\text{Fe(III)L}^3]^{3+}$ compound, both vertical lines indicate the anodic and cathodic potentials obtained under the conditions of study.

The voltamperogram (Fig. 35) was obtained starting from the potential of zero current and initiating the scanning in positive direction. For this complex, since with the L^3 ligand and the $[\text{Fe(DMSO)}_6]^{3+}$ ion it was observed that OD does not occur, the voltamperogram signals are attributed to oxidation and reduction of transition metal. In this case, an oxidation signal with an anodic peak potential $E_a = 0.5699 \text{ V/Ag-AgCl}$ is observed. When the scan is reversed, a reduction signal is observed with a cathodic peak potential $E_c = 0.2696 \text{ V/Ag-AgCl}$. The $E_{1/2}$ value for this system is 0.4197 V/Ag-AgCl .

5.6. Mechanism for the oxidative dehydrogenation reaction between L^2 and $[\text{Fe(DMSO)}_6]^{3+}$

The first step in the oxidative dehydrogenation reaction is the coordination of the L^2 ligand to the transition metal to form the compound $[\text{Fe(III)(L}^2\text{)(DMSO)}]^{3+}$. Which is formed by the displacement of 5 DMSO molecules by the Nitrogens of the ligand (Fig. 36)

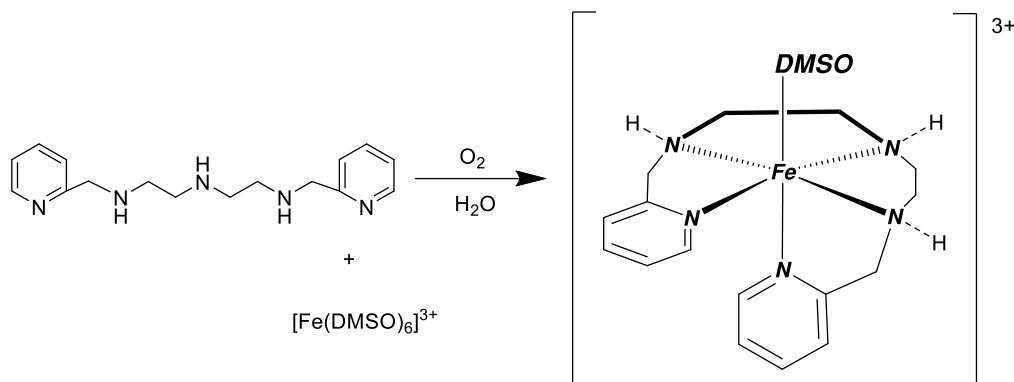


Fig. 36 First step in the oxidative dehydrogenation reaction L^2 and $[\text{Fe}(\text{DMSO})_6]^{3+}$.

Once the compound $[\text{Fe}(\text{III})(L^2)(\text{DMSO})]^{3+}$ is formed, a second step spontaneously occurs in which the Fe(II)-iminic compound $[\text{Fe}(\text{II})(L^4)(\text{DMSO})]^{2+}$ is formed (Fig. 37). The $\text{C}=\text{N}$ double bond conjugated to the pyridine ring stabilizes the Fe^{II} oxidation state because of its π acceptor capability.¹³

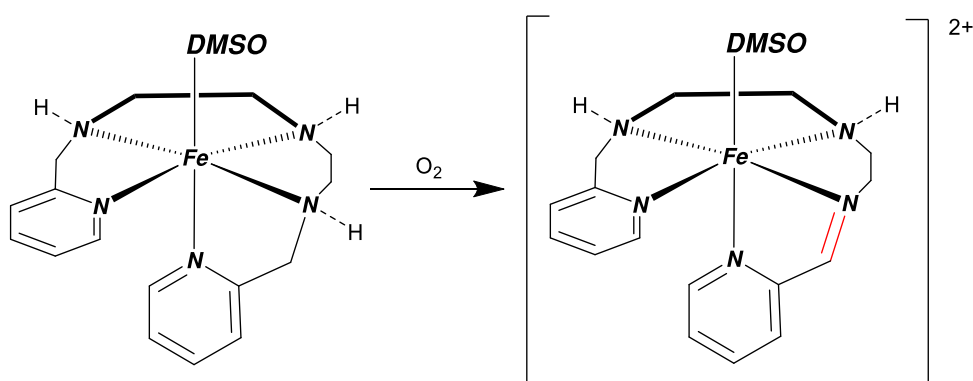


Fig. 37 Reduction of the ligand center and formation of the mono imine compound.

The product of the OD reaction has two characteristics, first the reduction of the transition metal and second the oxidation of the coordinated ligand. For the pentadentate ligand, however, studies have revealed that denticity in the final complex increases in primary and secondary amines in macrocyclic ligands. Cairns, McFall and Nelson²⁶ studied macrocyclic complexes, they mention the nucleophilic attack of solvent molecules (H_2O) to a $\text{C}=\text{N}$ imine type link of the coordinated molecule to the transition metal, which is stable in the presence of metal ions such as $\text{Fe}(\text{II})$. Since water was used as a solvent, it is proposed that the imine coordinated to $\text{Fe}(\text{II})$ would react with the solvent in the following manner to form a hexadentate ligand as proposed by Ugalde Saldívar²⁷ in his doctoral thesis.

First, the initial ligand with an imine bond and a Fe(II) atom undergoes a double attack by the solvent in the coordinated imine group giving rise to a *diol* (Fig. 38).

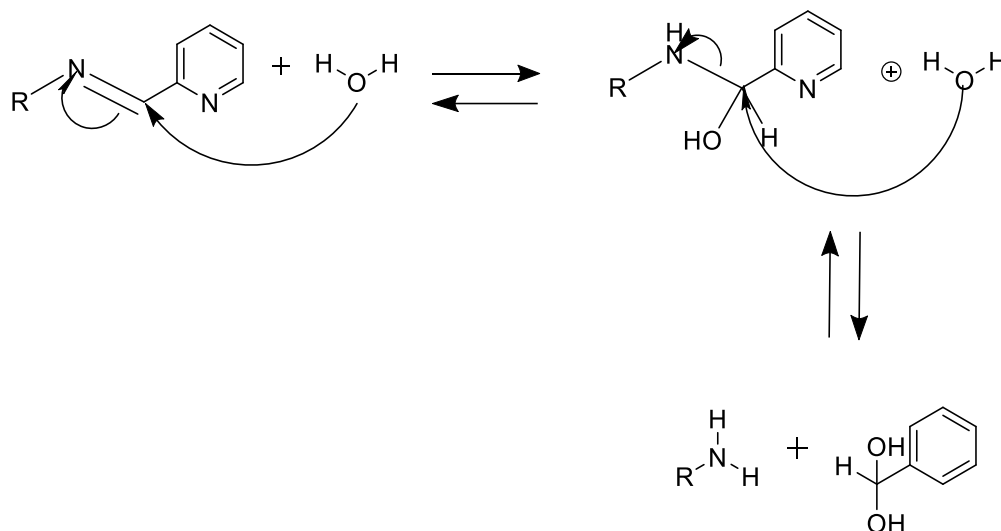


Fig. 38 *Diol* formation by nucleophilic attack of solvent molecules.

Then, the *diol* would react with another molecule of the proposed imine complex for which the central amine makes a nucleophilic substitution with a hydroxyl group of the *diol*, giving as a final product the hexadentate binder with the addition of a hydroxyl group plus a solvent molecule. (Fig. 39).

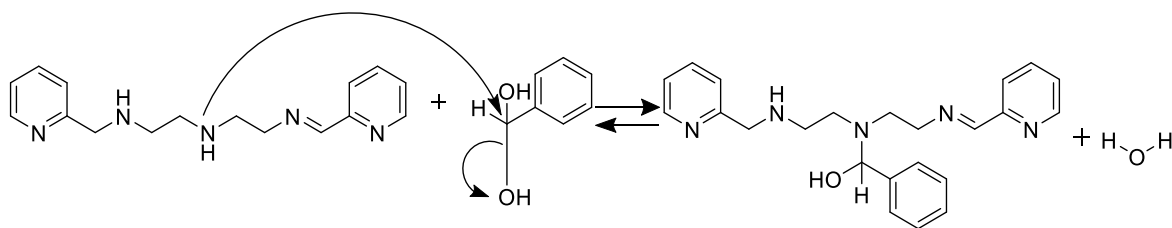


Fig. 39 Nucleophilic attack of the central imine ligand to the *Diol* for the formation of the new hexadentate ligand with the introduction of a hydroxyl group.

Therefore, after oxidative dehydrogenation, the following would occur (Fig. 40).

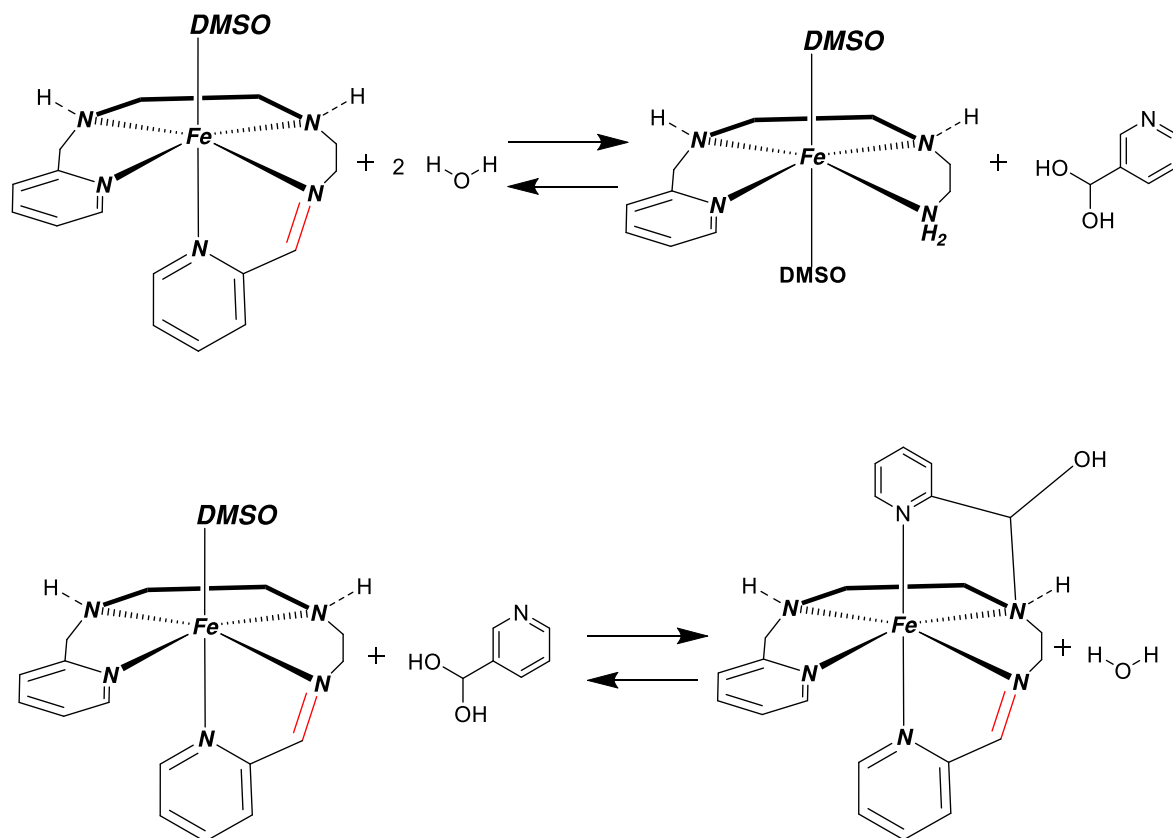


Fig. 40 General scheme of the formation of the finale hexadentate imine complex with the hydroxyl group.

Thus, the final product would be obtained with an increase in the ligand denticity plus the introduction of a hydroxyl group through the mechanism mentioned above.

5.7. Mechanism for the oxidative dehydrogenation reaction between L^3 and $[\text{Fe}(\text{DMSO})_6]^{3+}$

Data of cyclic voltammetry and the precipitation of the compound resulting from the reaction between L^3 and $[\text{Fe}(\text{DMSO})_6]^{3+}$ suggest that in this reaction oxidative dehydrogenation does not occur so the mechanism for the reaction would be as follows:

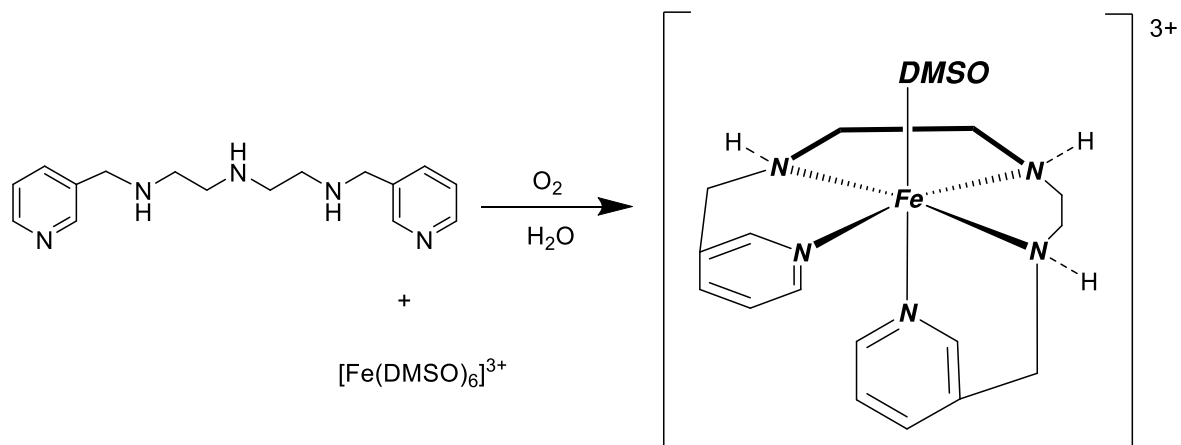


Fig. 41 L^3 ligand coordination to the Fe metal center to obtain the final compound $[\text{Fe}^{\text{III}}\text{L}^3(\text{DMSO})]^{3+}$.

Without OD in principle the reaction between the ligand and the complex would consist in the replacement of DMSO molecules by the ligand.

6. Summary and Conclusion

Two OD reaction systems between two trichlorohydrate ligands L^2 and L^3 and a $[\text{Fe}(\text{DMSO})_6](\text{NO}_3)_3$ complex were studied. The ligands were analyzed and characterized using IR, NMR spectroscopy and elemental analysis techniques which, due to their likeness, were very similar. An important finding was given in the analysis of their pKa, finding lower values for the L^2 . The importance of this result is that by finding a notable difference in the reactivity of both ligands even when they have a very similar structure, the parameter of the acidity of the proton of the amine can explain this difference in reactivity, that is, it is much easier to extract protons from L^2 , which leads to OD reaction.

The analysis of the magnetic susceptibility of the starting complex $[\text{Fe}(\text{DMSO})_6](\text{NO}_3)_3$ resulted in an effective magnetic moment (μ) of 5.73 BM which matches with a high spin Fe^{3+} molecule. The UV-Vis study in aqueous medium and by diffuse reflectance confirmed this result. Therefore, no transitions were observed in these spectra due to its prohibition by spin and by Laporte, since the baseline state for a high spin (d^5) Fe^{3+} is ${}^6\text{A}_{1g}$ and there is no excited state with that multiplicity.

The kinetics of the reaction between both ligands and the $[\text{Fe}(\text{DMSO})_6](\text{NO}_3)_3$ complex were followed by UV-Visible spectrophotometry in a range of 800 to 190 nm, resulting in rate constants values of $5.269 \times 10^{-5} \text{s}^{-1}$ for the reaction with L^2 and $1.4184 \times 10^{-4} \text{s}^{-1}$ for the reaction with L^3 . The lower order of magnitude between one reaction and another was attributed to the fact that the rate constant for the reaction with L^2 is influenced both by the coordination of the ligand to the metal and by the OD process. While the constant for the reaction with the L^3 is only influenced by its coordination to the metal, process much faster than the OD. Although the conditions were not optimal to observe all the expected spectral changes, by increasing the concentration between L^2 and the iron complex, it was possible to observe the appearance of two transitions, one in the range of visible at 576 nm and another in the UV range at 382 nm. This allowed to confirm a change in the electronic state of Iron in the new complex $[\text{Fe}(\text{II})L^4]^{2+}$ which was assigned to a change in the oxidation state of the iron from +3 to +2. For a low spin d^6 specie, according to the diagram of Tanabe Sugano five transitions are expected, while for a high spin specie only 1 transition is expected. This suggests a diamagnetic low spin d^6 species for the final complex. For the reaction with L^3 it was not possible to observe changes in its UV-Vis spectrum, this allowed to confirm that the oxidation state of the iron in this reaction did not change, and

since the reduction of the transition metal is indispensable for the OD it is confirmed that this process does not occur in this system.

The cyclic voltammetry carried out for the $[\text{Fe}(\text{DMSO})_6](\text{NO}_3)_3$ complex and the product of its reaction with L^2 ($\text{Fe}(\text{II})\text{L}^4$)²⁺ and L^3 ($\text{Fe}(\text{III})\text{L}^3$)³⁺, yielded a redox system for the first complex with a value of $E_{1/2} = 0.5206$ V/Ag-AgCl which was attributed to the oxidation and reduction of the transition metal (Fe) present in the system. For the ($\text{Fe}(\text{II})\text{L}^4$)²⁺ complex two redox systems were found, one with a value of $E_{1/2} = 0.4409$ V/Ag-Ag-Cl corresponding to the oxidation and reduction of transition metal, and a new redox system with a value of $E_{1/2} = 0.186$ V/Ag-Ag-Cl, which were assigned to the oxidation and reduction of the coordinated ligand, a characteristic process in OD reactions. For the ($\text{Fe}(\text{III})\text{L}^3$)³⁺ complex as well as for the $[\text{Fe}(\text{DMSO})_6](\text{NO}_3)_3$, only one redox system with a value of $E_{1/2} = 0.4197$ V/Ag-AgCl was found. The presence of a single system confirms the non-oxidation and reduction of the coordinated ligand. The change in $E_{1/2}$ potentials for iron oxide-reduction in the three species were attributed to the change in their coordination sphere.

These results, together with the literature review of previous works, allowed us to propose mechanisms for the reactions between both ligands and the iron complex. Thus, the $[\text{Fe}(\text{II})\text{L}^4]$ ²⁺ complex was obtained with a monoimine ligand with its increased denticity together with the introduction of a hydroxyl group. For the L^3 ligand, because the OD did not occur, the introduction of the pentadentate ligand to the metal coordination sphere was suggested as the final product by displacing the DMSO molecules. This was suggested because the increase in denticity and the introduction of the hydroxyl group, are favored by attack of solvent molecules (H_2O) to a C = N imine type link of the coordinated molecule to the transition metal, which is stable in the presence of metal ions such as Fe(II).

7. Bibliography

1. Housecroft CE, Sharpe AG. Inorganic Chemistry. In: Inorganic Chemistry. 2005. p. 765–6.
2. Cotton FA. Progress in Inorganic Chemistry. In: Progress in Inorganic Chemistry. 2009. p. 382.
3. Hartley FR. The cis- and trans-Effects of Ligands. *Chem Soc Rev.* 1973;2:163–6.
4. Su D, Qi W. Metal-free Carbon Catalysts for Oxidative Dehydrogenation Reactions. *ACS Publ.* 2014;4,9:3212–8.
5. LARGERON M, FLEURY M-B. A Biologically Inspired CuI /Topaquinone-Like Co-Catalytic System for the Highly Atom-Economical Aerobic Oxidation of Primary Amines to Imines. *Angewante Chemie.* 2012;51:5409–12.
6. Hamnett A. Mechanism and electrocatalysis in the direct methanol fuel cell. *Catal Today.* 1997;38(4):445–57.
7. Curtis NF. Macrocyclic coordination compounds formed by condensation of metal-amine complexes with aliphatic carbonyl compounds. *Coord Chem Rev.* 1968;3(1):3–47.
8. Keene FR. Metal-ion promotion of the oxidative dehydrogenation of coordinated amines and alcohols. *Coord Chem Rev.* 1999;187:122.
9. Curtis NF, Curtis YM, Powel HKJ. Transition-metal complexes with aliphatic Schiff bases. Part VIII. Isomeric hexamethyl-1,4,8,11-tetra-azacyclotetradecadienenickel(II) complexes formed by reaction of trisdiaminoethanenickel(II) with acetone. *Chem Soc A Inorganic, Phys Theor.* 1966;1015–8.
10. Keene FR, Lay PA, Sneddon GE, Whebell GW. Mechanism of Oxidative Dehydrogenation of an Amine Coordinated to Osmium(II). *Aust J Chem.* 1993;46:1763–5.
11. Taube H, Rudd DP. Disproportionation of ammine(pyridine)ruthenium(II) complexes in alkaline solution. *Inorg Chem.* 1971;10(7):1543.
12. Páez D. Efecto isotópico cinético del enlace C-H en reacciones de deshidrogenación

- oxidante de aminas promovida por hierro(III) bajo atmósfera de oxígeno. 2019.
13. Saucedo Vázquez JP, Kroneck PMH, Sosa Torres ME. The role of molecular oxygen in the iron(III)- promoted oxidative dehydrogenation of amines. *Dalt Trans.* 2015;44:5510–9.
 14. Driff A, Pineda A, Morvan D, Belliere-Vaca V, Jérôme F. Catalytic oxidative dehydrogenation of malic acid to oxaloacetic acid. *R Society Chem.* 2019;00:1–5.
 15. Scrosati B, Garche J. Lithium batteries: Status, prospects and future. *J Power Sources.* 2010;195(9):2419–20.
 16. Langford CH, Chung FM. On the Mechanism of Complex Formation and Solvent-Exchange Reactions of Iron(3+) in Dimethyl Sulfoxide. *Am Chem Soc.* 1968;90:4485–6.
 17. Ugalde-Saldívar VM, Sosa-Torres ME, Ortiz-Frade L, Bernés S, Höpfl H. Novel iron(II) complexes with hexadentate nitrogen ligands obtained via intramolecular redox reactions. *J Chem Soc Dalt Trans.* 2001;(20):3099.
 18. Wade L. G. *J. Organic Chemistry.* In 2013. p. 852.
 19. Mattson B, Anderso MP. *Micoscale Gas Chemistry.* 2017. p. 281–91.
 20. Tzou JR, Mullaney M, Norman RE. Hexakis(dimethyl suifoxide-O)iron(III) Trinitrate. *Acta Cryst.* 1995;C51:2249.
 21. Bain GA, Berry, Jhon F. Diamagnetic Corrections and Pascal’s Constants. *J Chem Educ.* 2008;85:533–5.
 22. Huheey JE, Keiter EA, Keiter RL. *Inorganic Chemistry Principles of Structure and Reactivity.* In 1993. p. 465.
 23. Espenson JH. *Chemical Kinetic and Reaction Mechanism.* In 1981. p. 13–29.
 24. Huheey JE, Keiter EA, Keiter RL. *Inorganic Chemistry Principles of Structure and Reactivity.* 1993;Fourth edi:391–432.
 25. Saucedo Vázquez JP. *Cinética de la Deshidrogenación Oxidativa de un Compuesto de Hierro con un Ligante Nitrogenado.* 2004.
 26. Cairns C, McFall SG, Nelson SM. Nickel(II) Complexes of Quinquedentate Macrocyclic

- Ligands and the Crystal and Molecular Structure of the Ring-opened Hydrolysis Product [1 1 -(6-Acetyl-2-pyridyl)-3,7,10-triazadodec-10-enylamine-NN'N''N'''-N''''] - aquanickel(II) Diperchlorate. *J Chem Soc, Dalt Trans.* 1979;(3):453.
27. Ugalde-Saldívar VM. Evaluación de la Reactividad de Compuestos de Hierro con el Ligante Picdien. 2002.
28. Huheey JE, Keiter EA, Keiter RL. *Inorganic Chemistry Principles of Structure and Reactivity.* In 1993. p. 540.
29. Huheey JE, Keiter RL, Keiter EA. *Inorganic Chemistry Principles of Structure and Reactivity.* 1993;Fourth edi:459–70.
30. Huheey JE, Keiter EA, Keiter RL. *Inorganic Chemistry Principles of Structure and Reactivity.* In 1993. p. 444.

8. Annexes

8.1. Substitution reactions in Square Planar Complexes

Metals with a d^8 electronic configuration usually are four coordinates and have square planar geometries, although, they can also be found in tetrahedral and octahedral geometries. The ligand substitution in square planar complexes can be made by nucleophilic substitution, electrophilic substitution and oxidative addition followed by reductive elimination.²

8.1.1. Nucleophilic substitution

Here we have an example of nucleophilic substitution reaction.

One step in the elucidation for a reaction is to determine the rate law of the substitution reaction experimentally.

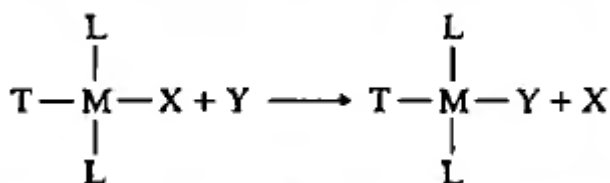


Fig. 1 General scheme of a substitution reaction taken from Huhhey.²⁸

We have a complex (Fig. 1.) in which Y is the nucleophilic entering ligand, X is the leaving ligand and T is the ligand *trans* to the leaving group. Chemist always try to simplify their kinetics experiments, an easy way to do that is to consider a pseudo first order reaction this means that the concentration of Y is made larger enough compared to that of the starting complex so that it appear that it remains constant over the time.²⁸ For reactions in which the reverse processes are insignificant the observed pseudo first order law for a square planar substitution is:

$$-\frac{d[\text{ML}_2\text{TX}]}{dt} = k_1[\text{ML}_2\text{TX}] + k_2[\text{ML}_2\text{TX}][\text{Y}] \quad (71)$$

Rearranging the equation is obtained that:

$$-\frac{d[\text{ML}_2\text{TX}]}{dt} = (k_1 + k_2\text{Y})[\text{ML}_2\text{TX}] = k_{\text{obs}}[\text{ML}_2\text{TX}] \quad (72)$$

Where

$$k_{\text{obs}} = (k_1 + k_2[\text{Y}]) \quad (73)$$

Non zero values for k_1 and k_2 from Eqs. 5-7 tell us that the reaction has two different pathways, the k_2 term first order with respect to the complex and $[Y]$, indicates an associative pathway, similar to the S_N2 reactions in organic chemistry. This term comes from the nucleophilic attack of the initial complex by Y . In a reaction in which bond making is important, here, rates of reaction depend on concentration and the nature of Y .

The k_1 term independent on Y would suggest at first a dissociative type substitution reaction. However, strong evidence suggest that this pathway is also associative. In general, the solvent (S) will be nucleophile and will compete with Y for the complex ML_2TX to form ML_2TS . Then, the rate law equation could be written as:

$$-\frac{d[ML_2TX]}{dt} = k'[ML_2TX][S] + k_2[ML_2TX][Y] \quad (74)$$

But, as the concentration of the solvent is in excess with respect to the complex and Y , this do not change over the time of the reaction and therefore, $k'[S] = k_1$

So, the two associative pathways could be seen as follows:

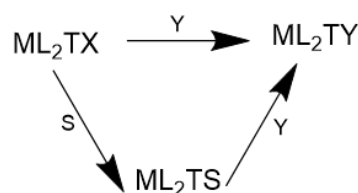


Fig. 42 General of scheme of the associative pathway in a substitution reaction.

, the k_1 term could also arise from the dissociation (D) of X to give a three coordinate complex that then will react with Y as follows:



Fig. 43 General Scheme of a dissociation reaction.

So, the rate law do not help to distinguish between an A or I_a or D and I_d mechanism for the k_1 pathway.

8.2. Magnetic Susceptibility

Explanation of the magnetic susceptibility showed below was taken from²⁹:

Substances can be classified as paramagnetics and diamagnetics. When substances are placed in an external magnetic field, there is an induced circulation of electrons producing a net magnetic moment, when this is aligned in opposition to the applied field substances are known as diamagnetics. This effect arises from paired electrons within a sample. Since all compounds contain paired electrons this is a universal property of matter.

On the other side, paramagnetism is produced by unpaired electrons. The spin and orbital motions of these electrons give rise to permanent molecular magnetic moments that tend to align themselves with an applied field.

When a substance is placed in a magnetic field, the field produced within the sample will either be greater than or less than the applied field, this difference can be expressed as:

$$\Delta H = B - H_0 \quad (75)$$

Where B is the induced field inside the sample and H_0 is the free field value.

Commonly, the difference between fields is expressed in terms of I , the intensity of the magnetization, which is the magnetic moment per unit volume:

$$4\pi I = B - H_0 \quad (76)$$

Since both B and I will tend to be proportional to the external field, dividing the last equation by H_0 , it will result in the ratios $\frac{I}{H_0}$ and $\frac{B}{H_0}$ that will be essentially constant for a given substance. The term $\frac{B}{H_0}$ is known as magnetic permeability while $\frac{I}{H_0}$ is the magnetic susceptibility per unit volume (k), which expresses the degree to which a substance is magnetizable.

$$4\pi k = \frac{B}{H_0} - 1 \quad (77)$$

The quantity that is most frequently obtained from experimental measurements of magnetism is the magnetic susceptibility per gram X_g , which is related to k through the density of the sample ($X_g = \frac{k}{d}$). By multiplying that amount by its molecular weight, we can obtain the molar susceptibility (X_M). This susceptibility value will contain the diamagnetic contributions in addition to the paramagnetic contributions, therefore, what is appropriate is to correct this value taking into account the sum of the diamagnetic contributions:

$$X_{\text{corr}} = X_{\text{M}} - \left(\sum \text{diamagnetic corrections} \right) \quad (78)$$

To relate the corrected magnetic susceptibility (X_{corr}) of the substance with the number of missing electrons in the molecule, the permanent magnetic moment (μ) is used.

8.3. Performance calculations for the yield of complex $[\text{Fe}(\text{DMSO})_6](\text{NO}_3)_3$ synthesis.

According to the synthesis reaction of $[\text{Fe}(\text{DMSO})_6](\text{NO}_3)_3$ (Fig.14) from $\text{Fe}(\text{NO}_3)_3 \cdot 9\text{H}_2\text{O}$ and DMSO, 1 mole of the iron complex reacts with 6 moles of DMSO for the synthesis of the final compound. Using 0.015 mols of $\text{Fe}(\text{NO}_3)_3 \cdot 9\text{H}_2\text{O}$ and 0.321 mols of DMSO it is obtained that the limiting reagent is the $\text{Fe}(\text{NO}_3)_3 \cdot 9\text{H}_2\text{O}$ and since one mole of this reagent produces one mole of the final complex, in the end 0.015 moles of $[\text{Fe}(\text{DMSO})_6](\text{NO}_3)_3$ should be obtained.

We have the following reaction:



Then we have that:

$$\begin{aligned} 0.015 \text{ mol } [\text{Fe}(\text{DMSO})_6](\text{NO}_3)_3 & * \frac{710.66 \text{ g } [\text{Fe}(\text{DMSO})_6](\text{NO}_3)_3}{1 \text{ mol } [\text{Fe}(\text{DMSO})_6](\text{NO}_3)_3} \\ & = 10.6599 \text{ g } [\text{Fe}(\text{DMSO})_6](\text{NO}_3)_3 \end{aligned} \quad (80)$$

The mass obtained was 9.1571 g, so the yield is equal to:

$$\text{yield} = \frac{9.1571 \text{ g}}{10.6599 \text{ g}} * 100\% = 85.90\% \quad (81)$$

8.4. Data tables for the pKa calculations

8.4.1. $\text{L}^2 \cdot 3\text{HCl}$

volume [ml]	pH	volume [ml]	pH
0	2,61	17,5	6,6

0,5	2,65	18,5	6,74
1	2,73	19	6,81
1,5	2,8	20	6,95
2	2,87	21	7,08
2,5	2,94	22	7,23
3	3,01	23	7,38
3,5	3,07	24	7,54
4	3,14	26	7,9
4,5	3,2	27	8,08
5	3,27	28	8,25
5,5	3,33	29	8,41
6,5	3,46	30	8,56
7	3,52	31	8,69
7,5	3,59	32	8,82
8	3,65	33	8,95
9	3,79	35	9,24
10	3,96	36	9,38
11	4,06	37	9,58
11,5	4,32	38	9,78
12	4,48	39	10,05
12,5	4,72	40	10,34
13	5,06	41	10,66
13,5	5,45	42	10,88

14	5,77	43	11,05
14,5	5,96	44	11,17
15	6,11	45	11,27
15,5	6,24	47	11,42
16	6,34	49	11,53
16,5	6,44	50	11,57
17	6,52		

Annex. 1 Data obtained for the titration curve of $L^2 \cdot 3HCl$ with NaOH

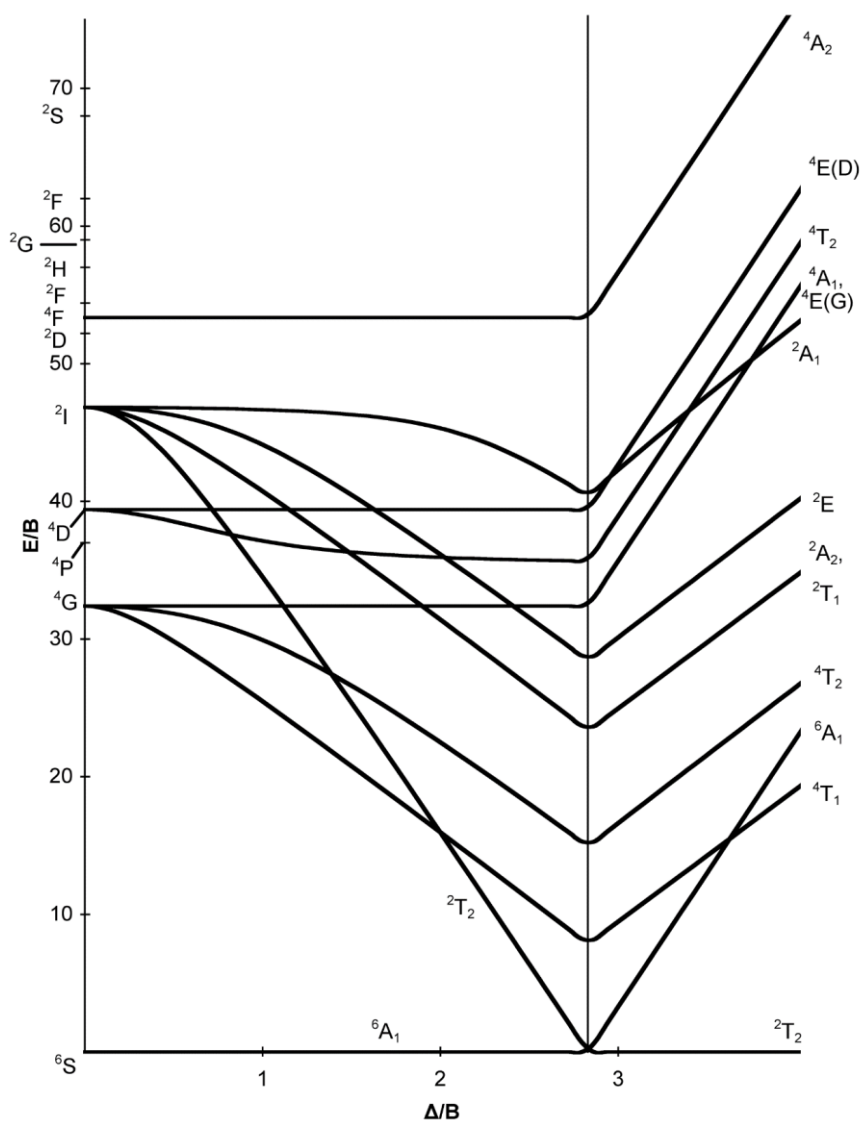
8.4.2. $L^3 \cdot 3HCl$

volume[ml]	pH	volume[ml]	pH
0	3,63	23	7,57
1	3,74	24	7,76
2	3,83	25	7,94
3	3,93	26	8,13
4	4,03	27	8,3
5	4,12	28	8,47
6	4,22	29	8,62
7	4,31	30	8,78
8	4,41	31	8,89
9	4,51	32	9,01
10	4,61	33	9,13
11	4,72	34	9,24

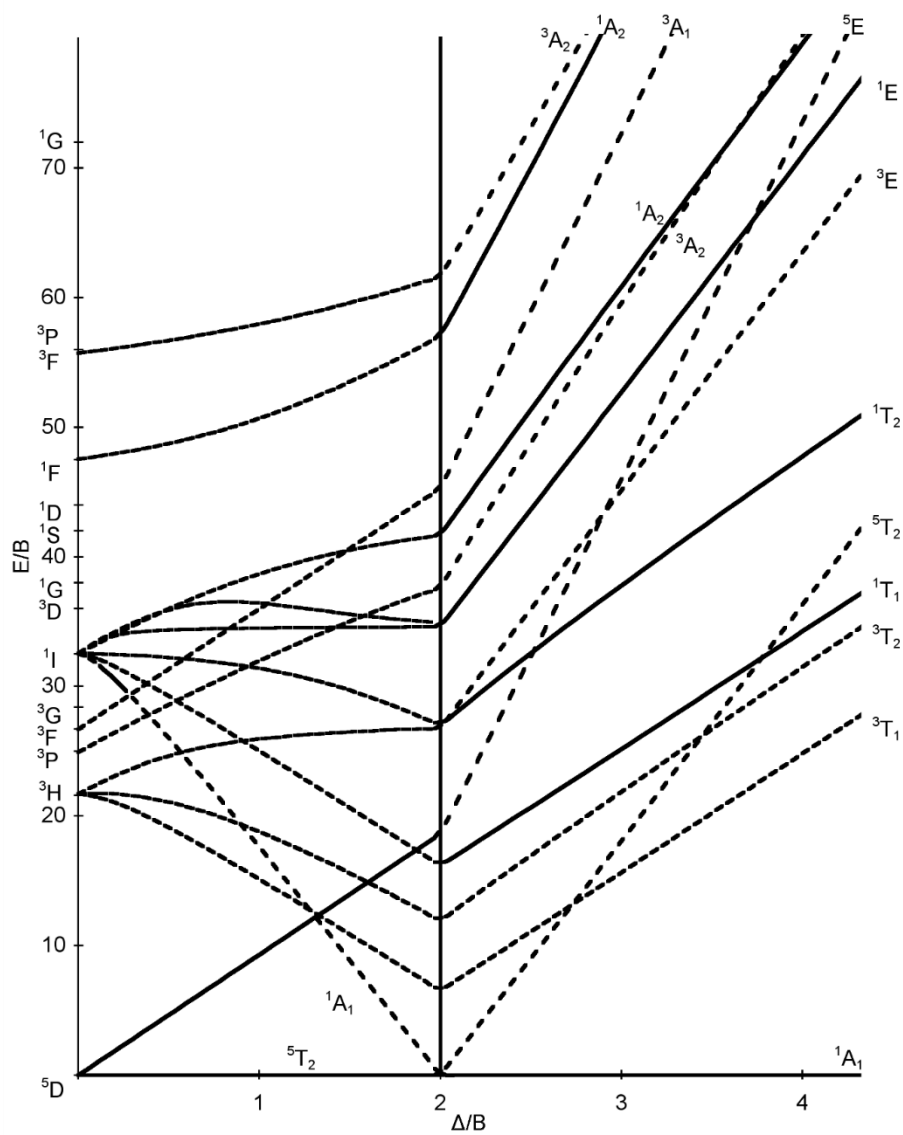
12	4,83	35	9,34
13	4,96	36	9,44
14	5,09	37	9,54
15	5,25	39	9,75
16	5,46	40	9,83
16,5	5,58	41	9,96
17	5,73	42	10,08
17,5	5,9	43	10,22
18	6,12	44	10,37
18,5	6,35	45	10,54
19	6,55	46	10,69
19,5	6,74	47	10,86
20	6,89	48	11
20,5	7,03	49	11,12
21	7,16	50	11,22
21,5	7,27	51	11,29
22	7,36	52	11,36
22,5	7,47	53	11,42

Annex. 2 Data obtained for the titration curve of $L^3 \cdot 3HCl$ with NaOH

8.5. Tanabe Sugano diagrams



Annex. 3 Tanabe Sugano diagram for a d^5 specie.



Annex. 4. Tanabe Sugano diagram for a d^6 specie taken from³⁰.